Discovery and therapeutic delivery of microRNAs targeting deregulated glioblastoma pathways inhibits tumor growth in mice

Shekhar Saha[#1], Ying Zhang[#1*], Myron K Gilbert Jr[#1], Collin Dube[#1], Farina Hanif[1,2], Elizabeth Qian Xu Mulcahy[1], Sylwia Bednarek[1], Yunan Sun[1], Pawel Marcinkiewicz[1], Xiantao Wang[3], Gijung Kwak[4,5], Ahsan Polash[3], Haolin Li[4,5,15], Kadie Hudson[1], Manikarna Dinda[6], Tapas Saha[7], Matthew McCord[8], Fadila Guessous[1,9], Nichola Cruickshanks[1], Rossymar Rivera Colon[1], Lily Dell'Olio[1], Rajitha Anbu[1], Wenjie Liu[1], Songy Choi[1], Benjamin Kefas[1,10], Pankaj Kumar[11], Alexander L Klibanov[12], David Schiff[13], Jung Soo Suk[4,5,14,15] Justin Hanes[16], Jamie Mata[17*], Markus Hafner[3*], Roger Abounader[1,13,18,19*]

Affiliations:

[1]Department of Microbiology, Immunology & Cancer Biology, University of Virginia School of Medicine, Charlottesville, VA 22908, USA.

[2]Department of Biochemistry, Dow International Medical College, Dow University of Health Sciences, OJHA Campus, SUPARCO Road, Karachi 74200, Pakistan.

[3]National Institute of Arthritis and Musculoskeletal and Skin Diseases, Bethesda, MD 20892, USA.

[4]Department of Neurosurgery, School of Medicine, University of Maryland, Baltimore, MD 21201, USA.

[5]Medicine Institute for Neuroscience Discovery (UM-MIND), School of Medicine, University of Maryland, Baltimore, MD 21201, USA.

[6]Department of Biochemistry and Molecular Genetics, University of Virginia School of Medicine, Charlottesville, VA 22908, USA.

[7]Swiss Re, Healthcare, Bengaluru, India.

[8]Department of Pathology, University of Virginia School of Medicine, Charlottesville, VA 22908, USA.

[9]Laboratory of Onco-Pathology, Biology and Cancer Environment, Faculty of Medicine, Mohammed VI University of Sciences and Health, Casablanca, Morocco

[10]Pharmacy, University of Virginia, Charlottesville, VA 22908, USA.

[11]Bioinformatics Core, University of Virginia School of Medicine, Charlottesville, VA 22908, USA.

[12]Cardiovascular Division, University of Virginia, Charlottesville, VA 22908, USA.

[13]Neurology, University of Virginia, Charlottesville, VA 22908, USA.

[14]Department of Neurosurgery, School of Medicine, Johns Hopkins University, Baltimore, MD 21205, USA.

[15]Department of Chemical and Biomolecular Engineering, School of Engineering, Johns Hopkins University, Baltimore, MD 21218, USA.

[16]Center for Nanomedicine at the Wilmer Eye Institute, Johns Hopkins University School of Medicine, 733 N Broadway, Baltimore, MD 21205, USA.

[17]Radiology and Medical Imaging, University of Virginia School of Medicine, Charlottesville, Virginia.

[18]NCI Designated Comprehensive Cancer Center, University of Virginia, Charlottesville, VA 22908, USA.

[19]Centre for RNA Science and Medicine, University of Virginia School of Medicine, Charlottesville, VA 22908, USA.

# Contributed equally

*Corresponding authors, ra6u@virginia.edu ,markus.hafner@nih.gov, jfm4q@virginia.edu, yz5h@virginia.edu

Abstract

Glioblastoma is a fatal primary malignant brain tumor, with an average survival of 15 months despite surgical resection, chemotherapy, and radiation therapy. Due to the concurrent deregulation of numerous genes in glioblastoma, molecular monotherapies have not improved clinical outcomes. Evidence suggests that targeting multiple deregulated molecules is essential for better therapies; however, this is limited by the lack of suitable drugs and increased toxicity of combination therapies. To address this, we hypothesized that miRNAs, small gene-regulatory RNAs that suppress mRNA, could simultaneously inhibit multiple deregulated genes in glioblastoma, and be used for more effective therapies. We identified regulatory miRNAs—those that target several deregulated genes in glioblastoma—using a combination of PAR-CLIP screening, TCGA data analyses and an algorithm to rank target importance and miRNA therapeutic potential. We selected two tumor suppressor miRNAs, miR-340 and miR-382, and one oncogenic miRNA, miR-17 and showed that they target critical glioblastoma pathways and alter cell growth, survival, invasion, and in vivo tumor growth. We developed and successfully applied a miRNA therapeutic delivery approach using Brain Penetrating Nanoparticles combined with MRI-guided focused ultrasound and microbubbles, to inhibit established tumor growth and to extend animal survival. This strategy offers a promising approach for translating miRNA-based therapies into clinical trials for glioblastoma and other cancers.

Introduction

Glioblastoma is an aggressive and fatal primary brain cancer that remains a formidable challenge due to its heterogeneity, therapeutic resistance, and invasive nature (1, 2) . Despite advances in therapies and clinical trials, the standard treatment of maximum surgical resection followed by radiation and temozolomide chemotherapy only extends patient survival to a modest 14.6 months (3-5). The Cancer Genome Atlas (TCGA) and other studies comprehensively analyzed deregulated gene expression in several hundred GBM tumors and described the concurrent deregulation of numerous genes in any single tumor (6, 7). Because of this multi-gene deregulation, molecular monotherapies have failed to achieve significant improvements in clinical outcomes. Several lines of evidence suggest that simultaneous targeting of several deregulated molecules is required to achieve better therapies (8, 9). However, the simultaneous targeting of several deregulated oncogenic drivers using conventional drugs is severely limited by the fact that the drugs needed to simultaneously target many deregulated molecules do not currently exist, and because combining several drugs in a clinical setting leads to an exponential increase in toxicity. The goal of this study was to identify regulatory microRNAs (miRNAs), defined as miRNAs that target several deregulated genes in glioblastoma, and deliver them or their inhibitors using what to our best knowledge is a new approach to simultaneously target multiple deregulated molecules for glioblastoma therapy.

MicroRNAs (miRNAs) are small non-coding RNA molecules that span 19-24 nucleotides. MiRNAs exert their effects by incorporating into argonaute (AGO) proteins (4 AGOs in

humans) and guiding them to target mRNA via seed-pairing predominantly to the 3'-untranslated regions (3'-UTR), and less commonly to the coding sequence (CDS), and 5'-untranslated regions (5'-UTR) of target genes. This facilitates the recruitment of effector proteins and the assembly of miRNA-induced silencing complexes (miRISC). The miRISC induces either mRNA degradation or translational inhibition (10). miRNAs play pivotal roles in regulating various cellular processes, including proliferation, invasion, apoptosis, and differentiation (11, 12). Dysregulation of miRNA expression is a hallmark of various cancer types, where miRNAs can function as either oncogenes or tumor suppressors by suppressing mRNAs of tumor suppressors or oncogenes, respectively (13-17). Importantly, because miRNAs do not require full complementarity to inhibit targeted mRNAs, single miRNAs can target and simultaneously inhibit numerous genes (18, 19).

We defined "regulatory miRNAs" as those that target several deregulated genes in glioblastoma. We reasoned that we could identify regulatory miRNAs and then use them for glioblastoma therapy. Using them as therapeutic agents would theoretically be equivalent to using a combination of several drugs that target deregulated glioblastoma driver genes. To find regulatory miRNAs, we first used PAR-CLIP to identify all targets of all miRNAs in glioblastoma cells (20). We then analyzed TCGA tumor data to determine which of these targets are deregulated in human tumors. We developed and implemented a computational algorithm to prioritize miRNA targets based on their relevance to glioblastoma malignancy. We selected the top candidate regulatory miRNAs, defined by

their capacity to regulate numerous target genes and therefore, exhibit strong anti-tumor effects when delivered as therapy.

A major challenge to successful miRNA therapy is delivery. The central nervous system's protective blood-brain barrier poses a formidable challenge to drug delivery. Focused Ultrasound (FUS) presents a noninvasive and reversible approach to transiently open the blood-brain barrier (BBB) in animal models. This temporary BBB opening facilitates drug delivery in brain tumors and other brain diseases (21). Recent clinical studies have successfully used Magnetic Resonance Image-guided FUS with microbubbles (MB) to deliver chemotherapeutic drugs to human brains and treat neurodegenerative conditions such as Alzheimer’s disease, Parkinson’s disease, and amyotrophic lateral sclerosis. A second challenge to achieving effective gene therapy distribution in the brain is the extracellular matrix (ECM), a dense and nanoporous network composed of electrostatically charged molecules such as proteoglycans, hyaluronan, and tenascins that restrict the diffusion of gene vectors through steric hindrance and adhesive interactions (22). To address this problem, brain-penetrating nanoparticles (BPN) consisting of poly(beta-amino esters) (PBAE) that are coated with a high density of polyethylene glycol (PEG) were developed (23).

In this study, we integrated miRNA target identification from PAR-CLIP with gene expression and survival data from TCGA to uncover regulatory miRNAs in glioblastoma. Through this integrative approach, we identified three key miRNAs that collectively regulate a substantial number of glioblastoma driver genes: miR-340 and miR-382, which

act as tumor-suppressive regulators targeting 87 and 79 genes respectively, and miR-17, which functions as an oncogenic regulator targeting 22 genes. We performed extensive functional assays with these regulatory miRNAs in glioblastoma cell lines and patient-derived stem cells and demonstrated their ability to inhibit cell proliferation, invasion, neurosphere formation, and xenografted tumor growth. Importantly, we also demonstrated that these miRNAs simultaneously targeted multiple glioblastoma-regulating genes in different pathways, decreasing their protein levels. We then used Magnetic Imaging-guided Focused Ultrasound (MRgFUS) in conjunction with microbubbles to transiently open the blood-brain barrier, enabling the local delivery of systemic PEG-PBAE BPNs carrying lentiviral plasmids encoding miR-340 and miR-382 to achieve upregulation of miR-340 and miR-382 in pre-established glioblastoma cell and stem cell xenografts. This approach significantly reduced glioblastoma in vivo growth and improved mouse survival. This work describes what we believe is a conceptually new approach to glioblastoma therapy to identify regulatory miRNAs and use MRI-guided FUS-MB and nanoparticles to deliver these microRNAs in vivo to inhibit glioblastoma growth. Given the availability of clinical grade FUS and BPN for brain applications, these findings pave the way for new miRNA therapeutic clinical trials.

Results

Identification of genome-wide miRNA targets in glioblastoma via PAR-CLIP.

Several online miRNA target prediction tools are available, but they can yield false positives and do not always capture all relevant targets. To identify regulatory miRNAs in glioblastoma, we therefore first used Photoactivatable Ribonucleoside-Enhanced Crosslinking and Immunoprecipitation (PAR-CLIP) to experimentally identify genome-wide targets for all miRNAs in glioblastoma cells (**Figure 1A**). PAR-CLIP was conducted in two biological replicates and independent experiments in U87 cells overexpressing either FLAG-tagged AGO1, AGO2, or AGO3. The cells were cultured in the presence of 4-thiouridine and the crosslinked RNA fragments bound by AGO1, AGO2, AGO3 were immunoprecipitated with anti-FLAG antibodies. Crosslinked RNAs were end-labeled using ^{32}P, and immunoprecipitates were fractionated by SDS-PAGE. Ribonucleoproteins (RNPs) were visualized by phosphorimaging, and the RNP corresponding to AGO was isolated and crosslinked RNA fragments recovered, reverse transcribed, and deep-sequenced. Sequence reads were mapped to the human genome and grouped into clusters using PARalyzer to identify those enriched in T-to-C mutations, which are induced by crosslinking of 4SU-containing RNA (**Figure 1B,C, Supplemental Figure 1A-E**). Resulting clusters of sequence reads were then analyzed to identify sites compatible with canonical seed pairing of miRNAs. We observed similar binding patterns for all three human AGO proteins (**Figure 1D,E**). A total of 19,483 clusters were obtained from the three AGO PAR-CLIP libraries, with 6,412 for AGO1, 7,007 for AGO2, and 6,064 for AGO3. 4,068 clusters were common across all three AGO samples (**Figure 1D, Table S1**). Among them, 279 mapped to 5′ untranslated regions (5′-UTRs), 4,635 to coding

sequences (CDSs), 4,750 to 3′ untranslated regions (3′-UTRs), and 513 to intronic regions (**Figure 1E, Supplemental Figure 1G-I**). These clusters correspond to 4,583 transcripts, representing approximately 23% of all protein-coding genes. A comprehensive list of mRNA targets for AGO1, AGO2, AGO3, along with their associated 611 expressed miRNAs, is provided in **Table S1**. These findings describe all mRNA targets of all miRNAs expressed in glioblastoma cells. They offer valuable insights into the genome-wide interactions between miRNAs and their targets in glioblastoma cells, illuminating the complex regulatory networks through which miRNAs modulate multiple targets.

Ranking of regulatory miRNAs based on the importance of their targets in human TCGA tumors.

Having identified all targets of all miRNAs in glioblastoma cells, we next sought to determine the relevance of these targets, and consequently of their targeting miRNAs, to glioblastoma malignancy. This process is described in the methods section (**Figure 1F**). Briefly, we analyzed The Cancer Genome Atlas (TCGA) data for the PAR-CLIP-identified miRNA targets in human tumors. We identified significantly deregulated targets (FDR ≤ 0.05) with a greater than 2-fold change in human tumors using the TCGA database. The targets were then scored based on the magnitude and frequency of dysregulation, as well as their correlation with patient survival, using a Cox coefficient threshold of 0.2 (**Figure 1G, Table S2 & S3**). Each target gene was assigned a composite score calculated from its absolute expression level in glioma samples and its fold change relative to normal brain tissue. These two metrics were independently converted into percentile ranks

(ranging from 0 to 1), and their sum represented the gene's composite score, with a theoretical range from 0 (lowest expression and change) to 2 (highest in both categories). For each miRNA, two aggregate scores were then computed: a tumor suppressor gene (TSG) score, representing the average composite score of its oncogenic targets, and an oncogene (ONC) score, reflecting the average composite score of its tumor suppressive targets. To enable comparison across the entire miRNA dataset, these scores were further normalized by converting them into percentile ranks across all miRNAs. To determine the functional role of each miRNA, we calculated the difference between its TSG and ONC percentile ranks. We then added the scores for each target and then added all scores for all targets of each miRNA. We subsequently averaged the target scores for both tumor suppressor and oncogenic miRNAs across the AGO1, AGO2, and AGO3 PAR-CLIP datasets, and consolidated the comprehensive set of targets for each miRNA (**Table S4 & S5**). The final score for each miRNA represents is potential regulatory and therapeutic potential because it is a reflection of both the number of its targets and the importance of these target in glioblastoma biology (**Table S6 & S7**).

Using this computational workflow, we identified several miRNAs that targeted many highly relevant genes that are dysregulated in GBM (**Figure 1H, Supplemental Figure 1F** and **Table S1-5)**. We designated these miRNAs as regulators because they can simultaneously target multiple significantly deregulated and biologically relevant genes and inhibit their expressions. This approach identifies miRNAs that are likely to exert strong therapeutic effects when delivered (tumor suppressive miRNAs targeting numerous oncogenes) or inhibited (oncogenic miRNAs that target numerous tumor

suppressors). The comprehensive list of miRNAs, their targets, and their scores can be found in **Table S1-7**.

Regulatory miRNAs miR-340 and miR-382 bind multiple targets and decrease their expression.

To prioritize regulatory miRNAs for functional validation, we incorporated evolutionary conservation as an additional criterion and selected the top five regulatory miRNAs from both the tumor suppressor (**Table S4**) and oncogenic (**Table S5**) lists for further analysis. Among these, we focused on two tumor-suppressive miRNAs, miR-340 and miR-382 because these miRNAs had high scores based on the algorithm described above. Our analysis determined that the tumor-suppressive regulatory miRNAs, miR-340 and miR-382, have 114 and 89 targets (**Table S4**), respectively. From these, we selected a subset for validation based on their known deregulation in glioblastoma and other cancers and their widespread expression in glioblastoma samples and patient-derived glioblastoma stem cells. We checked the expression of these selective targets, CD44, TOP2A, MDM2, RHOC, HMGA2, PLAU, and NUSAP1 in TCGA glioma patient samples and found that they are highly overexpressed in tumor samples compared with GTEx normal brain samples (**Supplemental Figure 2A-G**). We performed extensive target validation using immunoblot and 3'UTR reporter analyses. We transfected precursor miR-340 and miR-382 into glioblastoma cell lines A172, U87, U251, as well as patient-derived glioma stem cell lines GSC-34 and GSC-28. Cell lysates were then subjected to immunoblot. Overexpression of these miRNAs in various glioblastoma cells, and stem cells, led to a marked reduction in protein levels across all tested cell lines (**Figure 2A-L, Supplemental Figure 3A-I**). To determine if miR-340 and miR-382 directly target CD44,

TOP2A, RHOC, MDM2, HMGA2, EGFR, PDGFRA, NUSAP1, and PLAU by binding to their 3' untranslated regions (3'UTRs), we amplified the 3'UTR sequences containing the miR-340 and miR-382 binding sites from genomic DNA and cloned them into the psiCheck2 luciferase reporter plasmid under the control of the T7 promoter. These 3'UTR luciferase reporter constructs were then transiently transfected into U87 cells along with either a scrambled control miRNA mimic or mimics of miR-340 or miR-382. Overexpression of miR-340 resulted in a significant decrease in luciferase signals for CD44, RHOC, HMGA2, MDM2, EGFR, and PDGFRA ($p < 0.05$). Similarly, miR-382 overexpression led to a significant reduction in 3′UTR luciferase signals for PLAU, CD44, NUSAP1, and MDM2 ($p < 0.05$), compared to scrambled control transfections (**Figure 2M,N**). The predicted miRNA response elements (MREs) in these targets were identified based on 6-mer seed complementarity from PAR-CLIP analysis**.** Importantly, mutation of these seed-matching regions within the respective 3′UTRs abolished this repression, confirming the specificity of miR-340 and miR-382 targeting. These findings provide evidence that miR-340 and miR-382 directly bind to their respective 3′UTRs and significantly repress the expression of numerous deregulated genes in glioblastoma.

miR-17 is an oncogenic regulatory miRNA in glioblastoma.

We identified miR-17 as one of the top oncogenic regulatory miRNAs that targets several deregulated tumor suppressor genes in glioblastoma. We determined the expression of the selective targets in TCGA glioma samples and found they are highly downregulated in tumor samples compared with GTEx normal brain samples (**Supplemental Figure 4A-D**). We validated some of these targets using immunoblot analysis and 3’UTR reporter

assays in several glioma cell lines and patient-derived glioma stem cell lines. Since miR-17 is upregulated in glioblastoma and acts as an oncogene, we inhibited miR-17 by transfecting a miR-17 inhibitor into glioma cell lines (A172, U87, U251) and patient-derived glioma stem cell lines (GSC-28 and GSC-34). We selected specific targets—*ZBTB4, ANKRD11, EHD3,* and *EPHA4* based on their widespread published roles in glioblastoma. Inhibiting miR-17 resulted in an increased expression of all these targets in both glioblastoma cells and stem cells, indicating that miR-17 suppresses their expression (**Figure 3A-D, Supplemental Figure 5A-D**). To confirm that miR-17 directly binds to the 3'UTRs of ANKRD11, EHD3 and EPHA4 we conducted a luciferase reporter assay. The 3'UTR regions of these genes, which contain the miR-17 binding sites, were cloned into a psiCheck2 reporter plasmid. In addition, mutant constructs harboring point mutations in the predicted miR-17 seed-binding sites were generated. Glioblastoma cells were transfected with either a scrambled anti-miR or an miR-17 inhibitor, along with the luciferase reporter plasmid containing the wild-type or mutant miR-17 target binding sites. Transfection with the miR-17 inhibitor led to a significant de-repression (increase) in luciferase signals for ANKRD11, EHD3 and EPHA4 ($p < 0.05$), compared to the scrambled control (**Figure 3E**), whereas mutation of the binding sites abolished this effect. These data show that miR-17 directly binds to and regulates several deregulated mRNAs in glioblastoma.

Further, we investigated whether the targets of the regulatory microRNAs, miR-340, miR-382, and miR-17, are associated with patient survival. To evaluate survival outcomes, we utilized two independent cohorts of primary glioma patient samples from The Cancer

Genome Atlas (TCGA) and the Chinese Glioma Genome Atlas (CGGA) for survival analysis. Kaplan-Meier survival curves were generated and analyzed using the online tools GEPIA and CGGA, where patients were stratified into high and low gene expression groups based on target expression levels. For the tumor suppressor targets of miR-340 and miR-382, high expression was correlated with poorer patient survival, while low expression was associated with more favorable outcomes in both TCGA and CGGA cohorts (**Supplemental Figure 6A-G** & **Supplemental Figure 7A-G**). Conversely, for the oncogenic miR-17, high expression of its targets was linked to better survival, while low expression was associated with poorer patient prognosis (**Supplemental Figure 8A,B** & **Supplemental Figure 9A,B**). Additionally, we performed survival analysis using CGGA data from recurrent glioma patient samples, which revealed similar survival trends for both tumor suppressor and oncogenic miRNA targets (**Supplemental Figure 10A-F** & **Supplemental Figure 11**). These findings underscore the importance of regulatory miRNAs and their target genes in determining glioma patient outcomes.

Regulatory miRNAs miR-340 and miR-382 regulate multiple pathways in glioblastoma.

After identifying and validating regulatory miRNAs and their targets, we investigated their functions. We first performed pathway analyses with the targets of miR-340 and miR-382. We performed gene ontology (GO) term, Kyoto Encyclopedia of Genes and Genomes (KEGG), and hallmark pathway analysis. The most significant pathways associated with miR-340 were the mitotic cell cycle phase transition, stem cell differentiation, miRNAs in cancer, PI3K-Akt signaling, proteoglycan in cancer, the hallmarks of apoptosis, G2/M-

checkpoint and epithelial to mesenchymal transition (Supplemental **Figure 12A-C**). The pathways enriched for miR-382 targets were response to hypoxia, signaling pathways associated with miRNA metabolic process, proteoglycan in cancer, miRNAs in cancer, G2/M checkpoint, and epithelial to mesenchymal transition (Supplemental **Figure 12D-F**). These data suggest that these miRNAs regulate different cancer-related pathways and inhibiting them could attenuate glioma growth by inhibiting numerous oncogenic pathways.

Regulatory miRNAs miR-340 and miR-382 inhibit cell proliferation, invasion, and neurosphere formation in several glioblastoma cell lines.

We then performed a thorough assessment of the functional and experimental therapeutic impacts of miR-340 and miR-382. We first quantified their endogenous expression levels in glioblastoma cell lines, GSCs, and banked human tumors including cell lines (A172, T98G, LN18, U251, U87, SNB19), and stem cell lines (GSC-28, GSC-20, GSC-34, GSC-627, GSC-267), as well as patient glioblastoma samples, using quantitative PCR. Normal human astrocytes and normal human cortex were used as a control. We observed a significant downregulation of miR-340 and miR-382 expression in cell lines compared to normal human astrocytes, mirroring the pattern observed in patient glioblastoma samples compared to normal brain samples (**Supplemental Figure 13A-D**). Notably, miR-382 showed upregulation in only a single tumor tissue sample, while all other samples remained consistently downregulated. For miR-340, a majority of the cell lines showed downregulation, although a few cell lines exhibited relatively unchanged expression. These variations are consistent with the well-established intratumoral heterogeneity of

glioblastoma. This consistent downregulation hinted at a potential tumor suppressor role for these miRNAs, which was consistent with our analyses (**Supplemental Figure 13A-D**). Subsequently, we conducted cell proliferation and invasion assays to determine the biological significance of miR-340 and miR-382 *in vitro* across different glioblastoma cell lines. Glioblastoma cells were transfected with either scrambled control miRNA or precursor miR-340 or precursor miR-382, and cell proliferation was assessed through trypan blue staining and live cell counting. Overexpression of precursor miR-340 or miR-382 led to a significant reduction in cell proliferation compared to the scrambled negative control (**Figure 4A-D**). To investigate the influence of these miRNAs on glioma cell invasion, we performed transwell invasion assays using glioblastoma cell lines. The transwell invasion chambers were pre-coated with collagen IV, one of the abundant extracellular matrix components in the brain. Glioblastoma cell lines were transfected with scrambled control miRNA, or miR-340, or miR-382 precursors before being plated in the transwell chambers. These cells were allowed to invade through the collagen IV layer. Transient overexpression of either miR-340 or miR-382 led to a substantial reduction in glioblastoma cell invasion compared to scrambled negative control miRNA-transfected cells (**Figure 4E-J**).

Glioblastoma contains self-renewing stem cells contributing to tumor initiation and resistance to therapy (24). To elucidate the effect of the regulatory miRNAs on the self-renewal property of glioblastoma stem cells, we conducted neurosphere assays using two distinct patient-derived glioblastoma stem cell lines, GSC-34 and GSC-28. We transfected precursor miR-340 or precursor miR-382 or scrambled controls into the

glioblastoma stem cells and counted the number of neurospheres seven days post-miRNA-transfection. Neurospheres were categorized based on their size under the microscope (10 X magnification) into large, medium, and small groups. Overexpression of miR-340 and miR-382 resulted in a reduction in the total number of neurospheres in both GSCs. These findings suggest that these miRNAs impair neurosphere formation, potentially reflecting effects on self-renewal capacity (**Figure 4K–N**).

Inhibiting oncogenic miR-17 in glioma cells decreased cell proliferation, invasion, and neurosphere formation in glioblastoma cell lines and GSCs

miR-17 is one of the top oncogenic regulatory miRNAs identified by our integrated approach. Similar to the tumor suppressive regulatory miRNAs, we first checked the endogenous expression of miR-17 in multiple glioma and stem cell lines by RT-qPCR **(Supplemental Figure 13E,F)**. We observed an increased expression pattern in all glioma and stem cell lines consistent with our algorithm that identified miR-17 as an oncogenic miRNA. Therefore, we performed a series of functional assays with miR-17 in a spectrum of glioblastoma cell lines, including patient-derived glioblastoma stem cells. For the cell proliferation assay, we transfected the inhibitor against miR-17 into multiple glioma cell lines, and counted the cells on different days. We observed a decrease in cell proliferation supporting the oncogenic nature of miR-17 in glioma cells **(Figure 5A-C)**. Transwell cell invasion assays were carried out with miR-17 inhibitor in glioblastoma cell lines. The invasion assays were carried out with a collagen IV coated transwell chamber. Inhibition of miR-17 in glioblastoma cell lines led to a decrease in cell invasion through collagen-coated chambers, which were counted by taking images from five random

388 microscopic fields and quantified with ImageJ software (**Figure 5D-I)**. The neurosphere
389 formation assay was performed with glioma stem cell lines GSC-28 and GSC-34. The
390 transfection of glioma stem cell lines with an inhibitor of miR-17 decreases the overall
391 neurosphere formation. We categorized the neurosphere size into three different groups,
392 large, medium, and small, based on the size calculator with ImageJ software. The overall
393 neurosphere number in different categories decreased significantly after miR-17 inhibitor
394 treatment compared to the scrambled control treatment **(Figure 5J-M)**.
395
396 **Inhibition of Oncogenic miR-17 and Overexpression of Tumor-Suppressive miR-**
397 **340 and miR-382 reduce in vivo glioblastoma growth.**
398 The impact of miR-340 and miR-382 overexpression on xenografted tumor growth in mice
399 was investigated. We transfected $3x10^5$ U87 cells with either a scrambled negative control
400 miRNA (n=7), precursor miR-340 (n=7), precursor miR-382 (n=7), or miR-17 inhibitor
401 (n=7) **(Figure 6A)**. The transfected cells were then stereotactically implanted into the
402 striata of 6-week-old immunodeficient mice. Over three weeks, the mice were closely
403 monitored for tumor growth and survival, and MRI images were obtained to visualize the
404 tumors. After three weeks, the scrambled control U87 group exhibited significant tumor
405 growth. In contrast, the groups treated with miR-340 and miR-382 displayed a significant
406 reduction in tumor volume **(Figure 6B,C)**. Specifically, the scrambled control group
407 reached a tumor volume of (7.58 ± 2.26) mm^3, while the mice bearing miR-340- or miR-
408 382-transfected tumors showed tumor volumes of (4.59 ± 1.44) mm^3 and (2.86 ± 0.9)
409 mm^3, respectively (**Figure 6C**). The mice implanted with miR-17 inhibitor transfected cells
410 showed a substantial decrease in tumor volume compared to scrambled control **(Figure**

411 **6D,E)**. The scrambled control mice group showed tumor volumes of (5.3 ± 1.94) mm^3,
412 whereas miR-17 inhibitor group exhibited tumor volumes of 0.68 +0.29 mm^3. Collectively,
413 these *in vivo* findings support the use of miR-340, miR-382, the miR-17 inhibitor, or a
414 combination of them as new therapeutics for glioblastoma.
415
416 **Therapeutic delivery of PEG-PBABE brain penetrating nanoparticles (BPNs)**
417 **carrying plasmids encoding miR-340 and miR-382 to mice bearing glioblastoma**
418 **tumors by MRI-guided Focused Ultrasound inhibits tumor growth.**
419 For the therapeutic delivery of regulatory miRNA, we developed and employed an
420 approach consisting of MRI-guided focused ultrasound (MRgFUS) and microbubbles
421 (MB) (FUS-MB) to facilitate the delivery of BPNs carrying miR-340 and miR-382 encoding
422 lentiviral plasmids. This innovative approach (abbreviated FUS-MB-BPN) circumvents the
423 hurdles of miRNA therapeutics, particularly the blood-brain barrier and tumor penetration
424 and transfection, and delivers cargo loads to tumor cells. The schematic plan for FUS-
425 MB-BPN is depicted in **Figure 7A,B**. We generated glioblastoma xenografts in
426 immunodeficient mice, accomplished by intracranial implantation of $3x10^5$ U87 cells into
427 the striata of mice brains. Once the tumors had formed (7-10 days post-injection), we
428 verified tumor formation by MRI and the safe and effective opening of the blood-brain
429 barrier. This step was achieved through a meticulously orchestrated combination of
430 microbubbles and sonication, resulting in a conspicuous increase in MRI signal intensity
431 surrounding the tumors. This increased signal intensity is attributed to the leakage of the
432 MRI contrast agent, gadobenate dimeglumine, into the brain parenchyma after blood-
433 brain barrier opening (**Figure 7C**). To induce robust miRNA expression in brain tumors,

BPNs were formulated with lentiviral plasmids encoding miR-340 or miR-382. We also prepared the BPNs with plasmids encoding scrambled miRNA sequences as a control group. We extensively characterized these BPN particles because the zeta potential and size of the particles are important parameters for effective blood-brain barrier penetration. The hydrodynamic diameter and ζ-potential of BPNs carrying plasmids encoding scrambled miRNA, miR-340 and miR-382 were measured as 70.2 ± 4.7 nm, 2.8 ± 0.8 mV , 71.2 ± 1.2 nm, 2.3 ± 0.6 mV nm and 70.7 ± 1.0 nm and 1.8 ± 0.7 mV, respectively **(Table S8)**. After tumor implantation, we divided the brain tumor-bearing mice into two cohorts receiving plasmids encoding scrambled miRNA or tumor suppressive miR-340 and miR-382. Each group consisted of seven mice. The MRgFUS-MB + BPNs procedure was then executed. The BPNs carrying plasmids encoding scrambled miRNA or miR-340 or miR-382 were intravenously injected alongside microbubbles, and FUS was applied to the tumor regions to transiently open the BBB and facilitate the delivery of the plasmid cargoes into the tumor. One week after the FUS-MB-nanoparticles procedure, MRI images were taken to visualize and measure the tumor volumes. Delivery of miR-340 or miR-382 by FUS-MB-BPN into the tumors significantly reduced tumor burden compared to the control group (n = 7 mice per group, *=P<0.05). This represents to our best knowledge the first successful FUS-MB-BPN-based experimental therapeutic delivery of a miRNA to inhibit tumor growth (**Figure 7D,E**). We also closely monitored the post-FUS-treated mice for survival, which revealed that delivery of miR-340 or miR-382 into brain tumors significantly extended the survival of these mice compared to those treated with the scrambled control miRNA, with miR-382 providing greater survival benefit (**Figure 7F).** To determine whether the therapeutic efficacy of FUS-MB-BPN-mediated miRNA

delivery was restricted to U87 xenografts, we next extended our analysis to additional models. First, intracranial xenografts were established using patient-derived glioblastoma stem cells (GSC-34) and treated with the same FUS-MB+BPN protocol. Delivery of the tumor-suppressive miRNAs miR-340 or miR-382 significantly reduced tumor burden and improved survival relative to the scrambled control group (**Figure 7G–I**). To further evaluate treatment kinetics, longitudinal MRI was performed on days 4 and 7 post-FUS, revealing a progressive decline in tumor volume over time and thereby indicating sustained therapeutic efficacy (**Supplemental Figure 14A–D**). Importantly, delivery of BPNs carrying miR-340 or miR-382 in the absence of FUS did not produce a substantial reduction in tumor burden (FUS group: scrambled, miR-340, and miR-382: 64.81 ± 10.38, 15.65 ± 3.19, and 22.31 ± 9.99 mm^3, respectively; without FUS: 62.67 ± 11.97, 77.89 ± 14.67, and 72.09 ± 3.60 mm^3), highlighting the necessity of FUS-mediated BBB opening for effective tumor delivery (**Figure 7G-I and Supplementary Figure 15A–H**). Collectively, these findings demonstrate that FUS-MB-BPN-mediated delivery is broadly applicable across multiple glioblastoma models and effective for therapeutic miRNA delivery. To assess potential toxicity from FUS-MB, we harvested various organs, including the liver, kidney, brain, heart, spleen, lung, lymph nodes and pancreas from treated mice. We then performed H&E staining on these organs, which were analyzed by a neuropathologist. The data showed no apparent damage to the liver, kidney, brain, or heart in treated mice compared to the non-treated controls (**Supplemental Figure 16A,B**). These data demonstrate that FUS-MB-BPN is a safe and effective strategy for delivering miRNAs into brain tumors.

In vivo target repression and durability following MRI-guided FUS-mediated delivery of miR-340 and miR-382 to GSC-34 xenografts.

To determine whether the therapeutic effects observed following FUS-MB-BPN-mediated delivery of miR-340 and miR-382 were associated with effective and sustained repression of their molecular targets in vivo, we performed studies using GSC-34 glioma xenografts. Intracranial tumors were generated by implantation of GSC-34 cells into nude mice. After confirmation of tumor establishment by MRI, mice underwent MRI-guided focused ultrasound (FUS) in combination with microbubbles to transiently open the blood-brain barrier, followed by intravenous administration of BPNs carrying plasmids encoding miR-340, miR-382, or scrambled control miRNA. Tumor tissues were harvested at 4 and 7 days after FUS treatment for molecular analyses. Quantitative PCR analysis revealed significant downregulation of validated target transcripts for both miR-340 and miR-382 at 4 days post-treatment compared to scrambled controls (**Figure 8A-K**). While several targets showed robust repression at this early time point, a subset demonstrated more modest changes at day 4. Notably, by day 7, repression was consistently observed across all examined targets, indicating progressive and sustained transcript-level suppression following FUS-mediated miRNA delivery (**Figure 8A-K**). To determine whether transcript repression translated into functional protein downregulation, we analyzed protein expression in tumor lysates derived from the same GSC-34 samples. Western blot analysis at day 7 demonstrated marked reduction of validated on-target proteins in tumors treated with miR-340 or miR-382 relative to scrambled controls (**Figure 8L,M**). In contrast, expression levels of selected off-target proteins remained unchanged, supporting the specificity of miRNA-mediated repression in vivo (**Figure 8N**). Collectively, these data

demonstrate that FUS-MB-BPN delivery of miR-340 and miR-382 into GSC-34 brain tumors induces specific and durable suppression of molecular targets at both the mRNA and protein levels. The progressive repression observed between days 4 and 7 further supports sustained biological activity of the delivered miRNAs in vivo and provides molecular evidence underlying the observed antitumor effects.

Discussion

Glioblastoma is a lethal, and aggressive primary brain tumor. Despite extensive research and clinical trials, targeted therapies have faced insurmountable challenges presented by the blood-brain barrier, tumor invasiveness, resistance to cytotoxic therapies and tumor heterogeneity (25) . One major hurdle towards the success of targeted therapies for glioblastoma is the concurrent deregulation of numerous genes in any single tumor (14, 15). The simultaneous targeting of several deregulated oncogenic drivers using conventional drugs is severely limited by the fact that the drugs needed to simultaneously target many molecules do not currently exist, and because combining several drugs in a clinical setting leads to an exponential increase in toxicity (20). To overcome these limitations, we developed and successfully tested a new miRNA therapeutic strategy.

MicroRNAs are small noncoding RNAs that can be deregulated in cancers and brain tumors, where they can function as either oncogenes or tumor suppressors (26). Because miRNA do not require full complementary with the targeted mRNA sequences to inhibit gene expression, a single miRNA can target multiple genes and inhibit their expression (27). We therefore reasoned that there exist regulatory miRNAs, which can inhibit multiple deregulated genes in glioblastoma, and that these miRNAs can be used as therapeutic agents/targets, equivalent to using multiple drugs in combination (28). Combination drug therapies are difficult because many deregulated molecules do not have drugs that target them, and because combining several drugs can lead to exponential increase in toxicity (29, 30). Argonaute proteins AGO1–4 are core components of the RNA-induced silencing complex, but they differ functionally. AGO2 uniquely possesses endonucleolytic (“slicer”)

activity, while AGO1 and AGO3 primarily mediate translational repression and mRNA destabilization (31). In contrast, AGO4 is generally expressed at lower levels in most somatic tissues and has a less well-defined role in canonical miRNA-mediated silencing(32). Because AGO1–3 represent the predominant mediators of miRNA-guided repression in glioma cells, our PAR-CLIP analysis focused on these proteins to capture the major functional miRNA–mRNA interactions in this context. However, as these PAR-CLIP experiments were performed in U87 cells, the identified miRNA–mRNA interactions may not fully reflect the heterogeneity across glioblastoma subtypes. Future studies across additional patient-derived models will be important to establish the generalizability of these findings. To find regulatory miRNAs, we developed an approach that integrates miRNA target identification with PAR-CLIP with TCGA data analyses to find miRNAs that target multiple dysregulated important genes in glioblastoma. The initial PAR-CLIP experiments in U87 cells identified potential miRNA–target interactions, but these do not necessarily indicate the direction of miRNA dysregulation in patient tumors. Subsequent integration with TCGA data allows identification of miRNAs that are downregulated in glioma, reflecting the clinical context rather than the cell line expression. This unique approach was invented and developed in our lab and has not been described or published before. It can be applied to any human cancer.

Our approach uncovered numerous miRNAs that had numerous deregulated targets in glioblastoma. We focused on the highly ranked tumor suppressive miR-340 and miR-382 and the oncogenic miR-17. We validated a few of their targets, TOP2A, RHOC, CD44, HMGA2, MDM2 for miR-340 (**Figure 2A-G**) and CD44, NUSAP1, PLAU, and HMGA2 for

555 miR-382 targets **(Figure 2H-L)**, and ZBTB4, ANKRD11, EHD3, and EPHA4(**Figure 3A-**
556 **D**) for miR-17. These target genes were selected for validation based on prior evidence
557 from our GBM models, consistent expression across the cell lines used in this study, and
558 the availability of antibodies for Western blot analysis. Given the well-established
559 heterogeneity of glioblastoma, not all targets were uniformly expressed across all models;
560 therefore, we focused on representative and biologically relevant targets. Importantly, as
561 regulatory miRNAs act by coordinately regulating multiple genes within oncogenic
562 networks, their functional effects are driven by cumulative pathway modulation rather than
563 dependence on any single target (33-40). These selected targets were validated across
564 multiple cell lines, including patient-derived glioma stem cell lines, using immunoblotting
565 and 3'UTR reporter assays. CD44 is a cell surface adhesion protein highly expressed in
566 many cancers, including cancer stem cells, and regulates cancer progression and
567 metastasis (41). TOP2A has been identified as an oncogene in multiple cancers (34, 42).
568 TOP2A is overexpressed in pan-cancers, and overexpression is correlated with poor
569 prognosis and advanced pathological stages in most cancers (42). RhoC is a member of
570 the RhoGTPase family protein, which has been shown to be involved in cancer cell
571 migration, invasion, and metastasis (43). All selected targets are deregulated in
572 glioblastoma, where they play important roles in regulating malignancy. More targets were
573 identified and validated but are not all discussed in this section due to space limitations.
574 We then functionally validated the regulatory miRNAs by performing growth, death,
575 invasion, and differentiation assays as well as in vivo tumor growth assays. These assays
576 validated the tumor-suppressive (miR-340 and miR-382) or oncogenic (miR-17 potential)
577 effects of the selected regulatory miRNAs. We showed that the impact of these miRNAs

was pervasive and profound as illustrated in Figure 4A-F. While these functional assays support the tumor-suppressive or oncogenic roles of the selected miRNAs, we acknowledge that neurosphere formation assays were used to assess self-renewal capacity. Although informative, neurosphere assays are less quantitative than extreme limiting dilution assays (ELDA), which are considered the gold standard for estimating stem cell frequency. We recognize that reduced sphere formation may also be influenced by changes in proliferation rate, which cannot be fully distinguished in this assay system. In addition, we cannot exclude a contribution of altered cell viability to the observed effects. Given their ability to orchestrate concerted regulation of multiple pathways, we aptly designated miR-340, miR-382, and miR-17 as "regulatory miRNAs," and potential therapeutic agents or targets for glioblastoma therapy.

To translate these findings into therapy, we designed and tested an approach for the therapeutic delivery of miRNAs to glioblastoma animal models. We prepared BPNs carrying lentiviral plasmids encoding either miR-340 or miR282 or scrambled controls, and employed FUS-MB-BPN to deliver this therapeutic payload to mice harboring glioblastoma. This approach led to a significant reduction in tumor growth and prolongation of animal survival. The mice did not exhibit any signs of toxicity. This new noninvasive delivery method represents a pivotal step towards effective and targeted miRNA therapeutics. Efficient drug delivery into brain tumors is impeded by the blood-brain barrier (BBB). Utilizing MRI-guided Focused Ultrasound (MRIgFUS) combined with microbubbles provides a noninvasive technique to temporarily open the BBB for delivering therapeutic molecules with brain penetrating nanoparticles at the tumor site,

offering both temporal and spatial control (44-46). MRgFUS combined with microbubbles has been utilized in multiple studies to deliver therapeutic molecules into brain tumor (47). The blood brain barrier inhibits majority of chemotherapeutic drugs delivery into the brain including the chemotherapeutic drug doxorubicin (48). The polymeric nanoparticles have many advantages over cationic polymers such as polyethylenamine (PEI), poly-L-lysine (PLL) nanoparticles because they have more stability in the bloodstream, superior blood-brain barrier crossing potential, increased drug solubility and more drug encapsulated load and controlled drug release make them more suitable for delivering therapeutics when combined with MFgFUS. Among the promising polymers, poly(β-amino esters) (PBABEs) offer a library of nontoxic, biodegradable materials for the compaction of nucleic acids(49). In our study we used surface modified PEGylated PBAE nanoparticles which can penetrate brain parenchyma and open BBB efficiently when combined with microbubbles and FUS (49, 50). These blood brain penetrating nanoparticles are more diffusive in nature and were able to circulate in the brain at least for 24 hours suggesting they have low adhesive interactions with extracellular matrix that could lead to the clearance or low distribution of this particles in the brain parenchyma. The precision of focused ultrasound transducers enables them to focus on a millimeter scale, accurately targeting only the tumor region.

Recent advances in focused ultrasound (FUS)–mediated blood–brain barrier (BBB) disruption have rapidly transitioned from preclinical proof-of-concept toward clinical application in human glioblastoma. FUS, when paired with intravenously administered microbubbles, enables safe, targeted, and reversible BBB opening that enhances delivery

of chemotherapeutics, immunotherapies, and biologics to otherwise inaccessible tumor and peritumoral regions. Early clinical studies using MRI-guided FUS systems have demonstrated that repeated BBB disruption is feasible and well tolerated in patients with recurrent glioblastoma, with evidence of increased intratumoral drug penetration and favorable safety profiles (51, 52). Moreover, ongoing trials are assessing FUS-mediated delivery of standard agents such as temozolomide and new immune modulators, highlighting its potential to augment therapeutic efficacy. These developments position FUS as a versatile platform for improving CNS drug delivery and underscore the importance of integrating such technologies into translational frameworks for glioblastoma treatment.

In conclusion, our study developed and successfully tested approaches to identify and deliver therapeutic regulatory miRNAs to glioblastoma. This can be translated into clinical trials using the available clinical grade FUS-MB and BPN at our and other institutions. The approaches can also be easily adapted for use in other cancers as well.

Methods

Sex as a biological variable

Only male (or only female) mice were used in this study. This choice was made to reduce variability associated with sex-dependent hormonal differences and to improve experimental consistency in tumor growth models. Findings are expected to be generalizable to both sexes, although sex-specific effects were not directly evaluated.

Computational and experimental workflow for identifying putative regulatory miRNAs

Our new methodology for identifying key regulatory microRNAs (miRNAs) and their prioritization involved several steps. First, all miRNA mRNA targets were identified through PAR-CLIP **(described in more detail in the supplemental methods)**. Argonaute/target gene complexes were collected, the argonaute protein was digested, and the complexed target genes were then sequenced. T/C alignment analysis was used to identify genes with the distinctive mutation that identifies genes that complex with miRNAs. The sequence target fragments were then compared with a list of known miRNA seed sequences using string sequencing matching in R. Specifically, miRNAs that targeted genes in the 3'-untranslated region were prioritized, while genes with no miRNA matches or matches in the coding or 5'-untranslated regions were filtered out. Next, we analyzed 166 Glioblastoma Multiforme (GBM) RNA-Seq datasets from The Cancer Genome Atlas (TCGA), which were normalized against 255 normal brain datasets from the Genotype-Tissue Expression (GTEx, n = 255) project using the bowtie and bedtools genomic sequencing alignment packages. For 42,644 genes, these tumor samples were compared to normal using the DESeq2 package in R, revealing genes that were greater

than 2-fold up- and downregulated. Prior to downstream analyses, we implemented pre-filtering measures, discarding genes with read counts of less than five reads. In the third step, the CancerMine database was employed to classify each miRNA target gene as an oncogene (ONC), a tumor suppressor gene (TSG), or neither, using experimentally verified labels from published manuscripts. Using this method, the final curated repository contained 1849 published oncogenes and 1478 published tumor suppressors, a 1.25:1 ratio. The fourth step involved performing a survival analysis on the significantly deregulated genes from the previous differential expression analysis. Using the R programming package, survminer, a cox-proportional hazard ratio was determined for each putative target gene. The fifth step involved filtering out targets that did not have a "consistent" and "significant" survival and deregulation trend. For oncogenic targets, these parameters were determined as a minimum 2-fold increase in expression and a multiple hypothesis adjusted p-value of ≤0.05, coupled with either an inconclusive correlation with survival (cox coefficient between -0.2 and 0.2) or a correlation with poor prognosis (cox coefficient >0.2). Tumor suppressive targets required a minimum 2-fold decrease in expression, an adjusted p-value of ≤0.05, and either an inconclusive correlation with survival or a correlation with good prognosis (cox coefficient <-0.2). Targets that met these criteria were labeled "consistent" and were retained for the next step. For this sixth step, the retained "consistent" targets were assigned a composite score based on the percentile ranks of their absolute expression and differential expression scores. For example, a target at the 100th percentile would score 1, and at the 0th percentile would score 0, with the highest possible score being 2 for targets at the 100th percentile for both absolute and differential expression. Subsequently, each

686 miRNA received two scores reflecting the composite scores of their annotated targets: a
687 TSG score from oncogenic targets and an ONC score from tumor suppressive targets.
688 These scores were then ranked by percentile. In the final analysis, the percentile rank
689 difference between the TSG and ONC scores for each miRNA determined its
690 classification. The ONC percentile rank was subtracted from the TSG rank. A difference
691 exceeding 25% classified a miRNA as a TSG miRNA (TSG>ONC), while a difference
692 below -25% classified it as an ONC miRNA (ONC>TSG). This threshold was derived from
693 the 1.25:1 oncogene enrichment in our Cancermine dataset described in step three of
694 this analysis. For instance, miR-1185, with a TSG score in the 84th percentile and an
695 ONC score in the 12th percentile, was identified as a projected tumor suppressor miRNA
696 (+72% difference). This approach also minimized the emphasis on miRNAs targeting
697 numerous ONC and TSG genes, as they would rank highly in both categories. For
698 example, miR-4709 ranked in the 100th percentile for TSG and 90th percentile for ONC
699 but would receive "inconclusive" classification by our algorithm, as there is only a 10%
700 score difference in these roles.

701

702 **Photoactivatable-ribonucleoside-enhanced crosslinking and Immunoprecipitation**
703 **(PAR-CLIP)**

704 A total of 1 µg of FLAG-tagged AGO1, AGO2, AGO3 plasmids were transfected into
705 $2X10^5$ U87 cells via Lipofectamine 2000 transfection. Following transfection, the cells
706 were subjected to puromycin selection at a concentration of 1 µg/ml for 48 hours to
707 generate stable cell lines. Verification of AGO1, AGO2, AGO3 overexpression was
708 conducted through immunoblot analysis employing AGO1, AGO2, AGO3 antibodies. The

PAR-CLIP methodology was implemented and adapted from the previously established protocol (20). Briefly, AGO1, AGO2, AGO3 stable cell lines were cultured overnight in the presence of 100 µM 4-thiouracil (4SU), to label all cellular nascent RNA. Subsequently, these 4SU-labeled cells were exposed to 365 nm UV light (utilizing a Spectro Linker XL-1500) to effectuate the crosslinking of labeled nascent RNA with RNA binding proteins. Following UV exposure, cells were rinsed twice with 1X PBS, harvested, and lysed using a buffer composed of 50 mM HEPES-KOH (pH 7.5), 150 mM KCl, two mM EDTA (pH 8.0), one mM NaF, 0.5% NP-40, 0.5 mM DTT, and freshly prepared protease inhibitor cocktails. Cell lysates were centrifuged at 15,000Xg for 15 minutes at 4^0C. The supernatant from the lysed cells was subjected to treatment with RNAse T1 at a concentration of 1 U/µl for 15 minutes at room temperature. Subsequently, the Flag-tagged AGO1, AGO2, AGO3 cell lysates' supernatant underwent immunoprecipitation, facilitated by an anti-Flag antibody conjugated to Protein G Dynabeads. The immunoprecipitated material was further subjected to digestion with RNase T1, and the resulting beads were subjected to washing with a high salt wash buffer. The washed beads were re-suspended in a dephosphorylation buffer and treated with calf intestinal alkaline phosphatase for 10 minutes at 37^0C to eliminate phosphate groups from RNA molecules. Next, the dephosphorylated beads were treated with polynucleotide kinase and radioactive [γ-32P]-ATP for 30 minutes at 37^0C to introduce RNA labeling. The protein-RNA complexes were then separated via SDS-PAGE and subsequently electroeluted. These complexes exhibited a migration pattern at around 100 kDa. The electroeluted samples then underwent digestion with proteinase K to release RNA from the complexes, followed by RNA extraction involving an acid phenol/chloroform mixture

and ethanol precipitation. The extracted RNA was then converted into cDNA, and adaptor ligation was executed following previously established protocols (*31, 65*). The resulting libraries were sequenced, and the generated short reads were mapped against the human genome hg38, mRNA, and miRNA precursor databases and the clustered sequences were identified. The PAR-CLIP clustered sequences were identified by T to C conversion at the 4-thiouridine cross-linked site. The majority of the clustered sequences were found at the 3'-UTR regions. Finally, the true target sites were determined from the clustered sequences based on the list of input miRNA seed sequences.

DNA-Brain penetrating nanocomplexes (BPNs) synthesis and characterization

The preparation of BPN formulation was conducted in accordance with the protocol outlined in a previous publication(53). In summary, poly(beta-amino esters) (PBAE) and PEGylated PBAE (PEG-PBAE) were synthesized through the conjugation of 1,11-diamino-3,6,9-trioxaundecane (obtained from Millipore Sigma, St. Louis, MO) or 5 kDa methoxy-PEG-N-hydrosuccinimide (mPEG-NHS, 5 kDa, from Sigma-Aldrich) with the acrylate groups on PBAE (sourced from Sigma-Aldrich), respectively. The scrambled control miRNA (System Biosciences, catalog # PMIRH000PA-1), miR-340 (catalog # PMIRH340PA-1), and miR-382 (catalog # PMIRH382PA-1) lentiviral plasmids were purchased from System Biosciences (Palo Alto, CA, USA). All constructs are based on the pCDH-CMV-MCS-EF1-copGFP backbone, into which the respective precursor miRNA sequences were cloned according to the manufacturer's design. A mixture of PBAE and PEG-PBAE polymers was then prepared at a 3:2 ratio by PBAE amount to create a highly PEGylated surface. For the formulation of DNA-BPN, polymers and

nucleic acids were vigorously mixed at a weight ratio of 60 and a volume ratio of 1:5. This mixture was allowed to incubate at room temperature for 30 minutes to facilitate nanoparticle (NP) assembly. Subsequently, the solution was placed into 100 kDa MWCO Amicon Ultra Centrifugal Filters (Millipore Sigma) and centrifuged at 1,000 × g for 15 minutes at 4°C. To remove residual polymers from the DNA-BPN solution, the concentrated DNA-BPNs, with a nucleic acid concentration adjusted to 1 mg/mL, were diluted tenfold with DNase/RNase-Free Distilled Water and re-centrifuged under the same conditions. After undergoing two additional washing steps, the final DNA-BPN solution, with a nucleic acid concentration of 1 mg/mL, was prepared for subsequent in vivo experiments. The Physicochemical properties of BPN particles are described in **Table S8.**

MRI-guided Focused Ultrasound (MRIgFUS)

To establish tumors, immunodeficient mice aged 6-8 weeks were utilized. Specifically, $3X10^5$ U87 cells or GSC-34 patient-derived stem cells were intracranially introduced into the striata of immunodeficient mice. After a three-week injection period, MRI-guided focused ultrasound (MRIgFUS) was employed following a well-established protocol, with some modifications(54). Briefly, the MRIgFUS experimental setup featured an MRI-compatible pre-focused eight-element phased array, accompanied by a 1.5 MHz geometrically focused transducer boasting a 25 mm active diameter and a focal ratio of 0.8. These components were interconnected through a phased array generator and a radiofrequency power amplifier. It was connected to an MRI-compatible motorized stage to precisely control the transducer's movements in the rostral-caudal and medial-lateral

orientations. Degassed water was introduced into the spherical transducer's membrane to ensure effective coupling between the membrane and the mice's brains. At the same time, acoustic gel was applied to both the inflated membrane and the shaved portion of the mice's skull. These measures prevented the entrapment of air bubbles. For intravenous injections, a catheter was inserted into the mouse's tail. Microbubbles (25 µl/kg body weight) and an MRI contrasting agent, gadobenate dimeglumine (0.1 ml), were administered via this catheter with saline. Subsequently, a series of MRI images were captured. The precise positioning of the mouse's brain relative to the transducer was determined by locating the transducer's position within the MRI space. During sonication and MRI imaging, the mice were positioned in a prone posture. The region of interest (ROI) encompassing the tumor was defined, and sonication was carried out using a 1.5 MHz transducer to induce the opening of the blood-brain barrier around the tumor. MRI images were acquired using a surface coil incorporated into the FUS system. The effectiveness of blood-brain barrier opening was verified by comparing MRI sections before and after sonication. This MRI-guided focused ultrasound approach provided a powerful method for non-invasive modulation of the blood-brain barrier, enabling targeted delivery of therapeutic agents to brain tumors in preclinical models.

Detailed descriptions of all other methods can be found in the supplemental material

Statistical analyses

All data are represented as mean ± S.E.M. from three independent biological replicates. The P value is calculated by two tailed Student's t-tests when comparing two groups. P values of < 0.05 were considered statistically significant.

Study approval

Animal experiments were approved by the University of Virginia (Charlottesville, Virginia 22903) Animal Care and Use Committee (ACUC) (Protocol No. 3542-05-21). All animal procedures, including handling, monitoring, housing, and experimental interventions, were conducted in accordance with the guidelines of the National Institutes of Health and institutional ACUC regulations. Human glioma cell lines were used for intracranial implantation in mouse models.

Data and materials availability: The PAR-CLIP dataset generated in this study has been deposited in the Gene Expression Omnibus (GEO) under accession number GSE293517. All the data values are reported in the supporting data values file. All codes and materials supporting the findings of this study are available from the corresponding author upon reasonable request.

Acknowledgements

We thank Drs. Jeongwu Lee, Cleveland Clinic and Erik P. Sulman, NYU Langone Health for providing the glioblastoma stem cell lines GSC-28 and GSC-34 respectively. This work is supported by the University of Virginia Bioinformatics Core, Molecular Imaging Core, Advanced Microscopy Facility and Research Histology Core. We would also like to thank dbGAP and TCGA data management team for providing access to the raw RNA-seq data.

Funding support

This work is the result of NIH funding, in whole or in part, and is subject to the NIH Public Access Policy. Through acceptance of this federal funding, the NIH has been given a right to make the work publicly available in PubMed Central. NIH/NCI U01 CA220841, NIH/NINDS R01 NS122222, NIH/NINDS R21 NS122136, NCI Cancer Center Support Grant P30 CA044579, University of Virginia Comprehensive Cancer Center Pilot Grant, Schiff Foundation Grant, Ben and Catherine Ivy Foundation, and Focused Ultrasound Foundation.

Author Contributions

Conceptualization: SS, YZ, MKG, CD, RA

Methodology: SS, YZ, MKG, CD, FH, EQXM, SB, PM, XW, GK, KH, NC, RRC, FG, AP, HL, WL, SC, PK, ALK, JSS, JM

Investigation: SS, YZ, MKG, CD, RA

Visualization: SS, YZ, CD, MKG, FH, PM, MD, KH

Funding acquisition: RA

Project administration: RA

Supervision: RA

Writing – original draft: SS and RA

Writing – review & editing: all the authors

Competing interests: The authors declare there are no competing interests.

References

1. Bonavia R, Inda M-d-M, Cavenee WK, and Furnari FB. Heterogeneity maintenance in glioblastoma: a social network. *Cancer research.* 2011;71(12):4055-60.
2. Hoang-Minh LB, Siebzehnrubl FA, Yang C, Suzuki-Hatano S, Dajac K, Loche T, et al. Infiltrative and drug-resistant slow-cycling cells support metabolic heterogeneity in glioblastoma. *The EMBO journal.* 2018;37(23):e98772.
3. Stupp R, Dietrich P-Y, Kraljevic SO, Pica A, Maillard I, Maeder P, et al. Promising survival for patients with newly diagnosed glioblastoma multiforme treated with concomitant radiation plus temozolomide followed by adjuvant temozolomide. *Journal of Clinical Oncology.* 2002;20(5):1375-82.
4. Stupp R, Mason WP, Van Den Bent MJ, Weller M, Fisher B, Taphoorn MJ, et al. Radiotherapy plus concomitant and adjuvant temozolomide for glioblastoma. *New England journal of medicine.* 2005;352(10):987-96.
5. Calinescu A-A, Kamran N, Baker G, Mineharu Y, Lowenstein PR, and Castro MG. Overview of current immunotherapeutic strategies for glioma. *Immunotherapy.* 2015;7(10):1073-104.
6. Brennan CW, Verhaak RG, McKenna A, Campos B, Noushmehr H, Salama SR, et al. The somatic genomic landscape of glioblastoma. *Cell.* 2013;155(2):462-77.
7. Cancer Genome Atlas Research N. Comprehensive genomic characterization defines human glioblastoma genes and core pathways. *Nature.* 2008;455(7216):1061-8.

8. Debinski W. Drug cocktails for effective treatment of glioblastoma multiforme. *Expert Review of Neurotherapeutics.* 2008;8(4):515-7.
9. Shergalis A, Bankhead A, Luesakul U, Muangsin N, and Neamati N. Current challenges and opportunities in treating glioblastoma. *Pharmacological reviews.* 2018;70(3):412-45.
10. Djuranovic S, Nahvi A, and Green R. miRNA-mediated gene silencing by translational repression followed by mRNA deadenylation and decay. *Science.* 2012;336(6078):237-40.
11. Lawler S, and Chiocca EA. Emerging functions of microRNAs in glioblastoma. *Journal of neuro-oncology.* 2009;92(3):297-306.
12. Rupaimoole R, and Slack FJ. MicroRNA therapeutics: towards a new era for the management of cancer and other diseases. *Nature reviews Drug discovery.* 2017;16(3):203-22.
13. Chan JA, Krichevsky AM, and Kosik KS. MicroRNA-21 is an antiapoptotic factor in human glioblastoma cells. *Cancer Res.* 2005;65(14):6029-33.
14. Guessous F, Alvarado-Velez M, Marcinkiewicz L, Zhang Y, Kim J, Heister S, et al. Oncogenic effects of miR-10b in glioblastoma stem cells. *Journal of neuro-oncology.* 2013;112:153-63.
15. Kefas B, Godlewski J, Comeau L, Li Y, Abounader R, Hawkinson M, et al. microRNA-7 inhibits the epidermal growth factor receptor and the Akt pathway and is down-regulated in glioblastoma. *Cancer research.* 2008;68(10):3566-72.

16. Li Y, Guessous F, Zhang Y, DiPierro C, Kefas B, Johnson E, et al. MicroRNA-34a inhibits glioblastoma growth by targeting multiple oncogenes. *Cancer research.* 2009;69(19):7569-76.
17. Deforzh E, Uhlmann EJ, Das E, Galitsyna A, Arora R, Saravanan H, et al. Promoter and enhancer RNAs regulate chromatin reorganization and activation of miR-10b/HOXD locus, and neoplastic transformation in glioma. *Molecular cell.* 2022;82(10):1894-908. e5.
18. Selbach M, Schwanhäusser B, Thierfelder N, Fang Z, Khanin R, and Rajewsky N. Widespread changes in protein synthesis induced by microRNAs. *Nature.* 2008;455(7209):58-63.
19. Baek D, Villén J, Shin C, Camargo FD, Gygi SP, and Bartel DP. The impact of microRNAs on protein output. *Nature.* 2008;455(7209):64-71.
20. Hafner M, Landthaler M, Burger L, Khorshid M, Hausser J, Berninger P, et al. Transcriptome-wide identification of RNA-binding protein and microRNA target sites by PAR-CLIP. *Cell.* 2010;141(1):129-41.
21. McMahon D, O'Reilly MA, and Hynynen K. Therapeutic agent delivery across the blood–brain barrier using focused ultrasound. *Annual Review of Biomedical Engineering.* 2021;23:89-113.
22. Nance E, Timbie K, Miller GW, Song J, Louttit C, Klibanov AL, et al. Non-invasive delivery of stealth, brain-penetrating nanoparticles across the blood− brain barrier using MRI-guided focused ultrasound. *Journal of controlled release.* 2014;189:123-32.

912 23. Mead BP, Mastorakos P, Suk JS, Klibanov AL, Hanes J, and Price RJ. Targeted
913 gene transfer to the brain via the delivery of brain-penetrating DNA nanoparticles
914 with focused ultrasound. *Journal of Controlled Release.* 2016;223:109-17.
915 24. Osuka S, and Van Meir EG. Overcoming therapeutic resistance in glioblastoma:
916 the way forward. *The Journal of clinical investigation.* 2017;127(2):415-26.
917 25. Van Tellingen O, Yetkin-Arik B, De Gooijer M, Wesseling P, Wurdinger T, and De
918 Vries H. Overcoming the blood–brain tumor barrier for effective glioblastoma
919 treatment. *Drug Resistance Updates.* 2015;19:1-12.
920 26. Zhang B, Pan X, Cobb GP, and Anderson TA. microRNAs as oncogenes and
921 tumor suppressors. *Developmental biology.* 2007;302(1):1-12.
922 27. Peter M. Targeting of mRNAs by multiple miRNAs: the next step. *Oncogene.*
923 2010;29(15):2161-4.
924 28. Ghosh D, Nandi S, and Bhattacharjee S. Combination therapy to checkmate
925 Glioblastoma: clinical challenges and advances. *Clinical and translational*
926 *medicine.* 2018;7(1):33.
927 29. Mokhtari RB, Homayouni TS, Baluch N, Morgatskaya E, Kumar S, Das B, et al.
928 Combination therapy in combating cancer. *Oncotarget.* 2017;8(23):38022.
929 30. Scripture CD, and Figg WD. Drug interactions in cancer therapy. *Nature Reviews*
930 *Cancer.* 2006;6(7):546-58.
931 31. Liu J, Carmell MA, Rivas FV, Marsden CG, Thomson JM, Song J-J, et al.
932 Argonaute2 is the catalytic engine of mammalian RNAi. *Science.*
933 2004;305(5689):1437-41.

32. Meister G. Argonaute proteins: functional insights and emerging roles. *Nature Reviews Genetics.* 2013;14(7):447-59.
33. Mooney KL, Choy W, Sidhu S, Pelargos P, Bui TT, Voth B, et al. The role of CD44 in glioblastoma multiforme. *Journal of Clinical Neuroscience.* 2016;34:1-5.
34. Uusküla-Reimand L, and Wilson MD. Untangling the roles of TOP2A and TOP2B in transcription and cancer. *Science advances.* 2022;8(44):eadd4920.
35. Al-Kuraya K, Novotny H, Bavi P, Siraj AK, Uddin S, Ezzat A, et al. HER2, TOP2A, CCND1, EGFR and C-MYC oncogene amplification in colorectal cancer. *Journal of clinical pathology.* 2007;60(7):768-72.
36. Zhao Y, Yu H, and Hu W. The regulation of MDM2 oncogene and its impact on human cancers. *Acta Biochim Biophys Sin.* 2014;46(3):180-9.
37. van Golen KL, Wu Z-F, Qiao XT, Bao LW, and Merajver SD. RhoC GTPase, a novel transforming oncogene for human mammary epithelial cells that partially recapitulates the inflammatory breast cancer phenotype. *Cancer research.* 2000;60(20):5832-8.
38. Mansoori B, Mohammadi A, Ditzel HJ, Duijf PH, Khaze V, Gjerstorff MF, et al. HMGA2 as a critical regulator in cancer development. *Genes.* 2021;12(2):269.
39. Chen G, Sun J, Xie M, Yu S, Tang Q, and Chen L. PLAU promotes cell proliferation and epithelial-mesenchymal transition in head and neck squamous cell carcinoma. *Frontiers in genetics.* 2021;12:651882.
40. Hu Y, Xue Z, Qiu C, Feng Z, Qi Q, Wang J, et al. Knockdown of NUSAP1 inhibits cell proliferation and invasion through downregulation of TOP2A in human glioblastoma. *Cell Cycle.* 2022;21(17):1842-55.

41. Yan Y, Zuo X, and Wei D. Concise review: emerging role of CD44 in cancer stem cells: a promising biomarker and therapeutic target. *Stem cells translational medicine.* 2015;4(9):1033-43.
42. Wang X, Wang J, Lyu L, Gao X, Cai Y, and Tang B. Oncogenic role and potential regulatory mechanism of topoisomerase IIα in a pan-cancer analysis. *Scientific Reports.* 2022;12(1):11161.
43. Vega FM, Fruhwirth G, Ng T, and Ridley AJ. RhoA and RhoC have distinct roles in migration and invasion by acting through different targets. *Journal of Cell Biology.* 2011;193(4):655-65.
44. Chen P-Y, Hsieh H-Y, Huang C-Y, Lin C-Y, Wei K-C, and Liu H-L. Focused ultrasound-induced blood–brain barrier opening to enhance interleukin-12 delivery for brain tumor immunotherapy: a preclinical feasibility study. *Journal of translational medicine.* 2015;13:1-12.
45. Lamsam L, Johnson E, Connolly ID, Wintermark M, and Gephart MH. A review of potential applications of MR-guided focused ultrasound for targeting brain tumor therapy. *Neurosurgical focus.* 2018;44(2):E10.
46. Wu S-K, Tsai C-L, Huang Y, and Hynynen K. Focused ultrasound and microbubbles-mediated drug delivery to brain tumor. *Pharmaceutics.* 2020;13(1):15.
47. Ishida J, Alli S, Bondoc A, Golbourn B, Sabha N, Mikloska K, et al. MRI-guided focused ultrasound enhances drug delivery in experimental diffuse intrinsic pontine glioma. *Journal of Controlled Release.* 2021;330:1034-45.

48. Treat LH, McDannold N, Zhang Y, Vykhodtseva N, and Hynynen K. Improved anti-tumor effect of liposomal doxorubicin after targeted blood-brain barrier disruption by MRI-guided focused ultrasound in rat glioma. *Ultrasound in medicine & biology.* 2012;38(10):1716-25.

49. Kim J, Mondal SK, Tzeng SY, Rui Y, Al-Kharboosh R, Kozielski KK, et al. Poly (ethylene glycol)–poly (beta-amino ester)-based nanoparticles for suicide gene therapy enhance brain penetration and extend survival in a preclinical human glioblastoma orthotopic xenograft model. *ACS biomaterials science & engineering.* 2020;6(5):2943-55.

50. Fields RJ, Cheng CJ, Quijano E, Weller C, Kristofik N, Duong N, et al. Surface modified poly (β amino ester)-containing nanoparticles for plasmid DNA delivery. *Journal of controlled release.* 2012;164(1):41-8.

51. Zhu H, Allwin C, Bassous MG, and Pouliopoulos AN. Focused ultrasound-mediated enhancement of blood–brain barrier permeability for brain tumor treatment: a systematic review of clinical trials. *Journal of neuro-oncology.* 2024;170(2):235-52.

52. Chen K-T, Lin Y-J, Chai W-Y, Lin C-J, Chen P-Y, Huang C-Y, et al. Neuronavigation-guided focused ultrasound (NaviFUS) for transcranial blood-brain barrier opening in recurrent glioblastoma patients: clinical trial protocol. *Annals of Translational Medicine.* 2020;8(11):673.

53. Mastorakos P, Zhang C, Song E, Kim YE, Park HW, Berry S, et al. Biodegradable brain-penetrating DNA nanocomplexes and their use to treat malignant brain tumors. *Journal of Controlled Release.* 2017;262:37-46.

54. Chen P-Y, Hsieh H-Y, Huang C-Y, Lin C-Y, Wei K-C, and Liu H-L. Focused ultrasound-induced blood–brain barrier opening to enhance interleukin-12 delivery for brain tumor immunotherapy: a preclinical feasibility study. *Journal of translational medicine.* 2015;13(1):93.

Figure Legends

Figure 1: Identification and prioritization of regulatory miRNAs in glioblastoma: A) Schematic overview of PAR-CLIP. B) The phosphorimage of SDS-PAGE gel of RNA-Argonaute (Ago) complexes labeled with 5′-32P that were immunoprecipitated with a Flag-tag antibody. The complex is expected to appear near 100 kDa. C) Agarose gel separation of PCR products from AGO1, AGO2, AGO3 PAR-CLIP cDNA libraries. D) A Venn diagram illustrating the overlap in miRNA clusters identified with AGO1, AGO2, AGO3. E) Venn diagram showing the distribution of identified targets in 3'-UTR regions from AGO1, AGO2 and AGO3 PAR-CLIP. F) Diagram depicting the algorithm used for determining regulatory miRNAs in glioblastoma. G) Volcano plot denoting the statistically significant miRNAs based on Cox Proportional Hazard. H) Classification of miRNAs as oncogenic and tumor-suppressive based on their targets derived from AGO1, AGO2, AGO3 PAR-CLIP.

Figure 2: Validation of miR-340 and miR-382 targets in glioblastoma cells and patient-derived stem cells: A-L) Glioblastoma cell lines A172, U87, U251, and patient-derived stem cell lines GSC-28 and GSC-34 were transfected with either a scrambled negative control, miR-340, or miR-382. Immunoblots were probed with antibodies against TOP2A , RHOC , CD44 , HMGA2, MDM2, CD44, NUSAP1, PLAU, and HMGA2. GAPDH served as the internal loading control. The data show that miR-340 and miR-382 downregulated protein expression compared to negative controls. M,N) 3'UTR luciferase activity assays in U87 cells were performed by co-transfecting cells with miR-340 (M) or

miR-382 (N) and a psiCheck2 luciferase reporter plasmid containing the wild-type 3'-UTR regions of target genes CD44, TOP2A, RHOC, HMGA2, MDM2, EGFR, and PDGFRA (M), or PLAU, CD44, NUSAP1, HMGA2, and MDM2 (N), along with corresponding mutant 3'-UTR constructs in which the predicted miRNA binding sites were disrupted. The data show that miR-340 and miR-382 decreased luciferase activity for all respective wild-type targets compared to controls, while this repression was abolished or significantly reduced in the mutant constructs. Data represent mean ± SEM from three independent experiments. Statistical significance was determined using a two-tailed Student's t-test, with *= $P<0.05$.

Figure 3: Validation of miR-17 targets in glioblastoma cells and patient-derived stem cells: A-D) Glioma cell lines A172, U251, GSC-28, and GSC-34 were transfected with a miRNA inhibitor targeting miR-17. Immunoblots were performed with antibodies against ZBTB4, ANKRD11, EHD3, and EPHA4. GAPDH served as the internal control for loading. The data show that the miR-17 inhibitor increased protein expression compared to negative controls. E,F) U87 cells were co-transfected with miR-17 or miR-17 inhibitor along with psiCheck2 luciferase reporter plasmids containing the wild-type 3'-UTR regions of targets ANKRD11, EHD3, EPHA4, and ZBTB4, as well as corresponding mutant 3'-UTR constructs in which the predicted miR-17 binding sites were disrupted. The data show that the miR-17 inhibitor increased luciferase activity for all respective wild-type 3'UTR targets compared to negative controls, while this effect was abolished or significantly reduced in the mutant constructs. Forty-eight hours after transfection, cells

were lysed and luciferase signals were measured. Data represent mean ± SEM from three independent experiments. *=P<0.05.

Figure 4: miR-340 and miR-382 inhibit cell proliferation, invasion, and neurosphere formation in glioblastoma: A-D) Glioblastoma cell lines U87 and U251 were transfected with either a scrambled control, or miR-340, or miR-382. Cell counts were performed at various time points, and miR-340 and miR-382 showed decreased cell growth compared to negative controls. E-J) A172, U87, and U251 cells were transfected with mimic miR-340 and miR-382 and invasion assays were executed. Invaded Images from 5-10 random fields were captured and analyzed using ImageJ software for quantification. miR-340 and miR-382 decreased invasion compared to negative controls K-N) Six-well plates were pre-coated with poly-ornithine, and glioblastoma stem cell lines GSC-28 and GSC-34 were plated and transfected with either scrambled control miRNA, miR-340, or miR-382. Neurosphere images were taken from five distinct fields 72 hours post-transfection and categorized into large, medium, and small using ImageJ software, with quantifications presented in (M, N). miR-340 and miR-382 decreased neurosphere formation compared to negative controls. Data represent mean ± SEM from three independent experiments. *=P<0.05.

Figure 5: Effects of miR-17 inhibition on cell proliferation, invasion, and neurosphere formation in glioblastoma: A-C) A172, U87, and U251 were transfected with either scrambled control miRNA or a miR-17 inhibitor. Cells were counted 48 hours

post-transfection using trypan blue exclusion at various intervals to assess viability. D-I) A172, U87, and U251 cells were transfected with control or miR-17 inhibitor. Invasion assay was carried out and the invaded cells were stained with crystal violet, and images were captured and analyzed using ImageJ software for quantification. J-M) Glioma stem cell lines GSC-28 and GSC-34, plated on poly-ornithine-coated 6-well plates, were transfected with either a scrambled control miRNA or an miR-17 inhibitor. Neurospheres were imaged 72 hours post-transfection in the neurobasal complete growth medium. Images from five different microscopic fields were taken, and neurosphere sizes were categorized into large, medium, and small for quantification using ImageJ software. Data are presented as mean ± SEM from three independent experiments. *=P<0.05.

Figure 6: miR-340, miR-382 and miR-17 regulate in vivo tumor growth: A) Schematic overview of the experimental design for tumor implantation and timeline for MRI imaging to assess tumor volume. Each group comprised seven mice for surgery. B-E) U87 cells were transfected with scrambled negative miRNA, miR-340, miR-382, or an inhibitor of miR-17. 48 hours post-transfection, cells were implanted intracranially into the striata of 5-6-week-old immunodeficient mice. Mice were monitored for 3-4 weeks, and MRI imaging was performed to evaluate tumor generation. Representative MRIs and quantification showing that miR-340, miR-382 and miR-17 inhibitor showed reduction in tumor volume compared to Scramble controls. *=P<0.05.

Figure 7: Inhibition of in vivo glioma growth through MRI-guided (MRIg) Focused Ultrasound, Microbubbles and Brain-Penetrating Nanoparticles (FUS-MB-BPN) delivery of miR-340 or miR-382: A) A schematic representation of FUS-MB-BPN-mediated miRNA delivery into mice. B) Overall experimental plan and timeline for FUS-MB-BPN. C) Tumors in mice were sonicated pre and post FUS-MB-BPN, and images were captured to validate blood-brain barrier opening. MB were employed to facilitate blood-brain barrier opening. Arrows indicated the tumor location and show dispersion of the contrast demonstrating successful opening of the blood-brain barrier. D,E) Microbubbles were injected through the mice's tail vein, and MRIgFUS was conducted. Upon confirmation of blood-brain barrier opening, BPN conjugated with either scrambled, miR-340 or miR-382 were injected through the mice's tail vein. The mice were imaged using MRI, and tumor volume shows significant reduction upon delivery of miR-340 or miR-382 compared to Scramble controls at day 15. F) Kaplan Meir survival curve showing miR-340 or miR-382 significantly prolonged survival compared to scrambled control mice. G–I) For patient-derived glioma stem cell (GSC-34) intracranial xenografts, the same FUS-MB-BPN protocol was applied using miR-340 and miR-382. MRI analysis at day 4 and day 7 post-FUS showed a reduction in tumor volume over time, and Kaplan–Meier survival analysis demonstrated improved survival in miR-340- and miR-382-treated groups compared to scrambled controls. n = 7 mice per group. *=P < 0.05. n = 7 mice per group. *=$P < 0.05$ for miR-340-treated vs. scramble control.

Figure 8: In vivo target repression and durability following MRI-guided focused ultrasound–mediated delivery of miR-340 and miR-382 in GSC-34 glioma

xenografts: (A–K) Quantitative PCR analysis of validated target transcripts demonstrates significant downregulation in tumors treated with miR-340 or miR-382 compared to scrambled controls at day 4, with more uniform and sustained repression observed at day 7. While some targets exhibited modest suppression at day 4, consistent transcript-level repression across all examined targets was evident by day 7, indicating progressive and durable in vivo silencing following FUS-mediated delivery. (L–M) Western blot analysis of tumor lysates at day 7 confirms reduced protein expression of validated on-target genes in miR-340– and miR-382–treated tumors relative to controls. (N) Expression of selected non-target proteins remains unchanged, supporting specificity of miRNA-mediated repression. Statistical significance was determined using a two-tailed Student's t-test. *=P< 0.05.

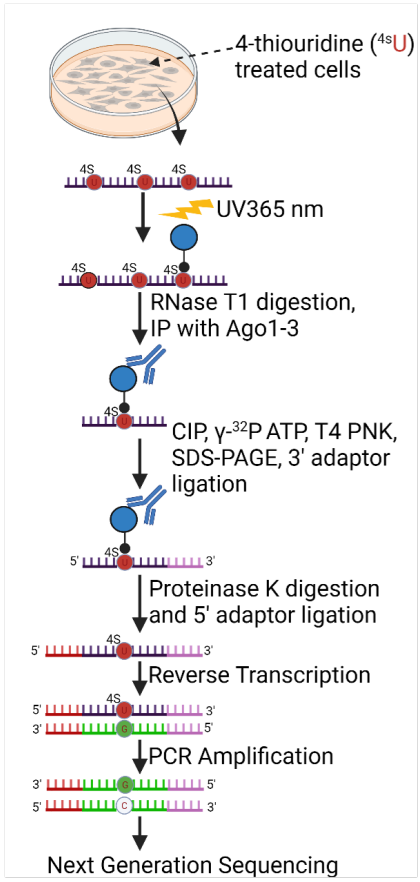
A
4-thiouridine (4sU) treated cells
UV365 nm
RNase T1 digestion, IP with Ago1-3
CIP, γ-32P ATP, T4 PNK, SDS-PAGE, 3' adaptor ligation
Proteinase K digestion and 5' adaptor ligation
Reverse Transcription
PCR Amplification
Next Generation Sequencing

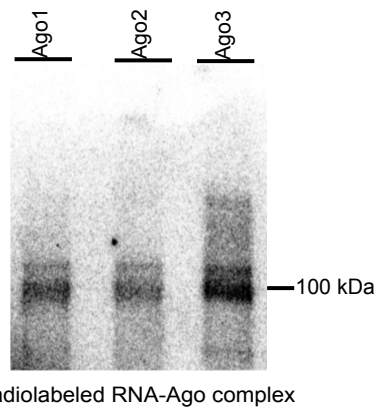
B
Ago1
Ago2
Ago3
100 kDa
5'-radiolabeled RNA-Ago complex

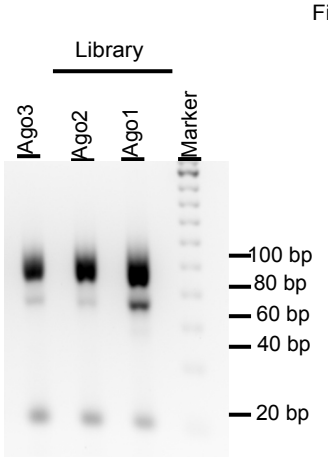
C
Library
Ago3
Ago2
Ago1
Marker
100 bp
80 bp
60 bp
40 bp
20 bp


D
AGO1
AGO2
AGO3
409
1547
807
4068
388
585
1023

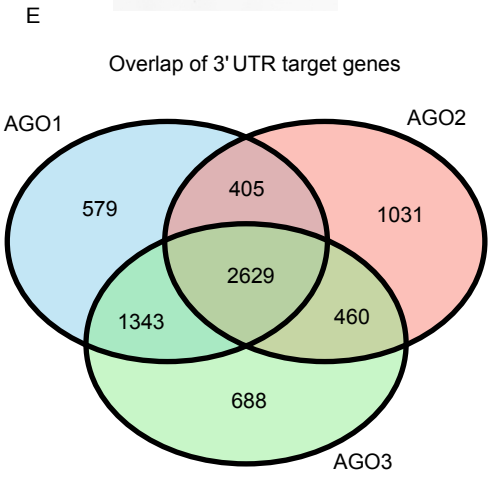
E
Overlap of 3' UTR target genes
AGO1
AGO2
AGO3
579
405
1031
2629
1343
460
688

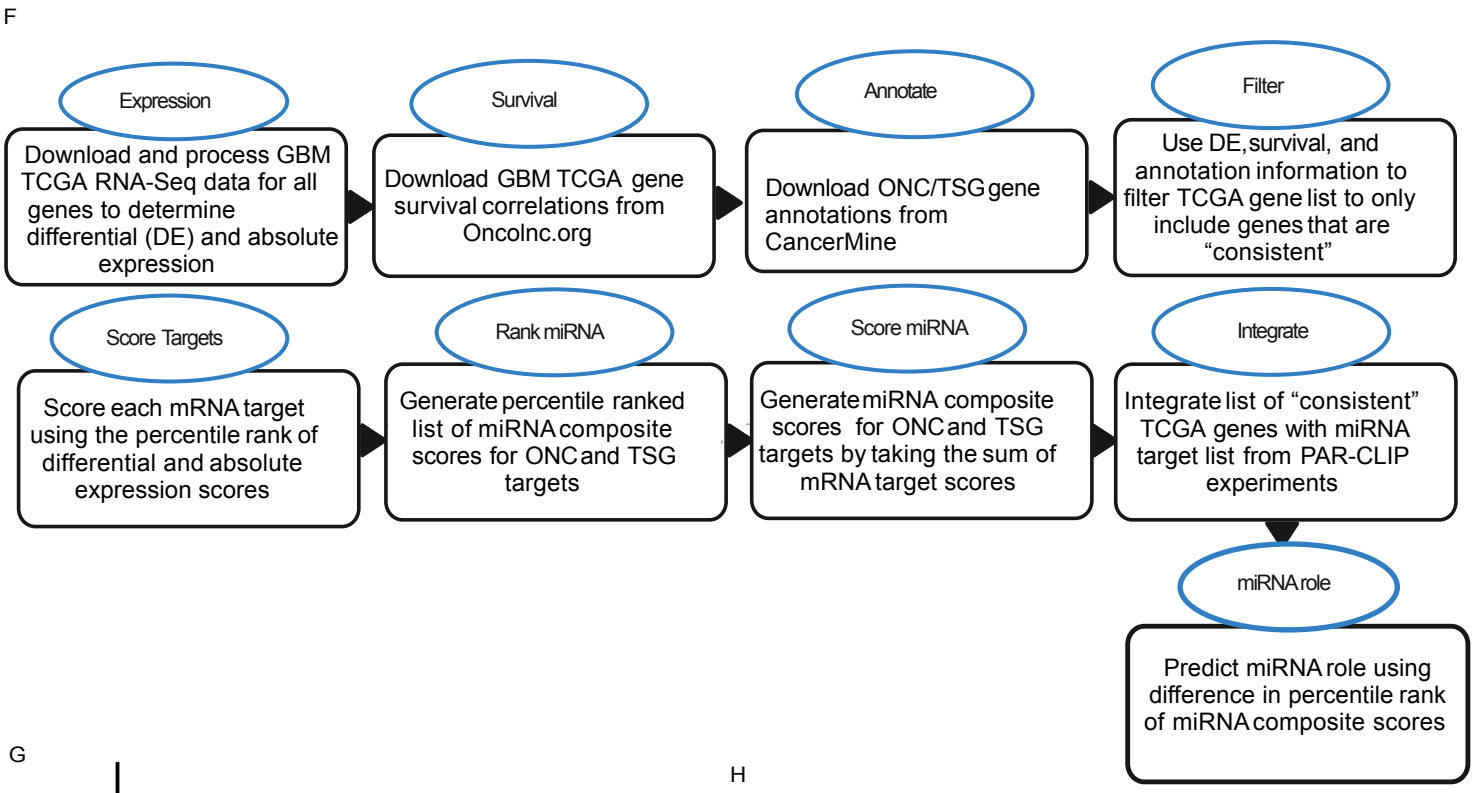
F
Expression
Download and process GBM TCGA RNA-Seq data for all genes to determine differential (DE) and absolute expression
Survival
Download GBM TCGA gene survival correlations from Oncolnc.org
Annotate
Download ONC/TSG gene annotations from CancerMine
Filter
Use DE, survival, and annotation information to filter TCGA gene list to only include genes that are "consistent"
Score Targets
Score each mRNA target using the percentile rank of differential and absolute expression scores
Rank miRNA
Generate percentile ranked list of miRNA composite scores for ONC and TSG targets
Score miRNA
Generate miRNA composite scores for ONC and TSG targets by taking the sum of mRNA target scores
Integrate
Integrate list of "consistent" TCGA genes with miRNA target list from PAR-CLIP experiments
miRNA role
Predict miRNA role using difference in percentile rank of miRNA composite scores

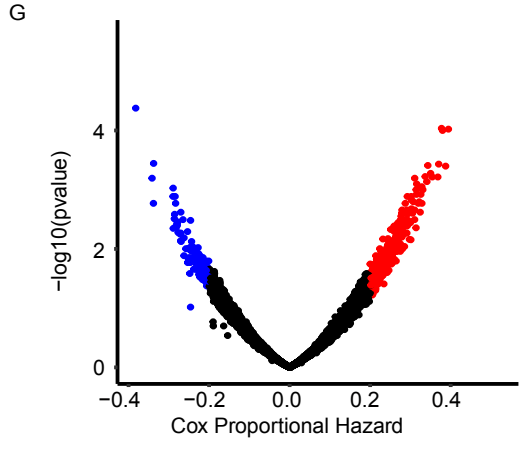
G
−log10(pvalue)
Cox Proportional Hazard

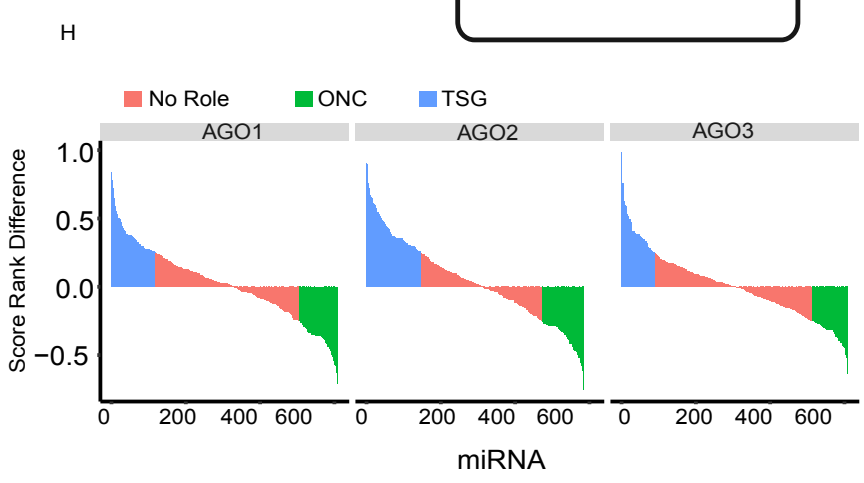
H
No Role
ONC
TSG
AGO1
AGO2
AGO3
Score Rank Difference
miRNA

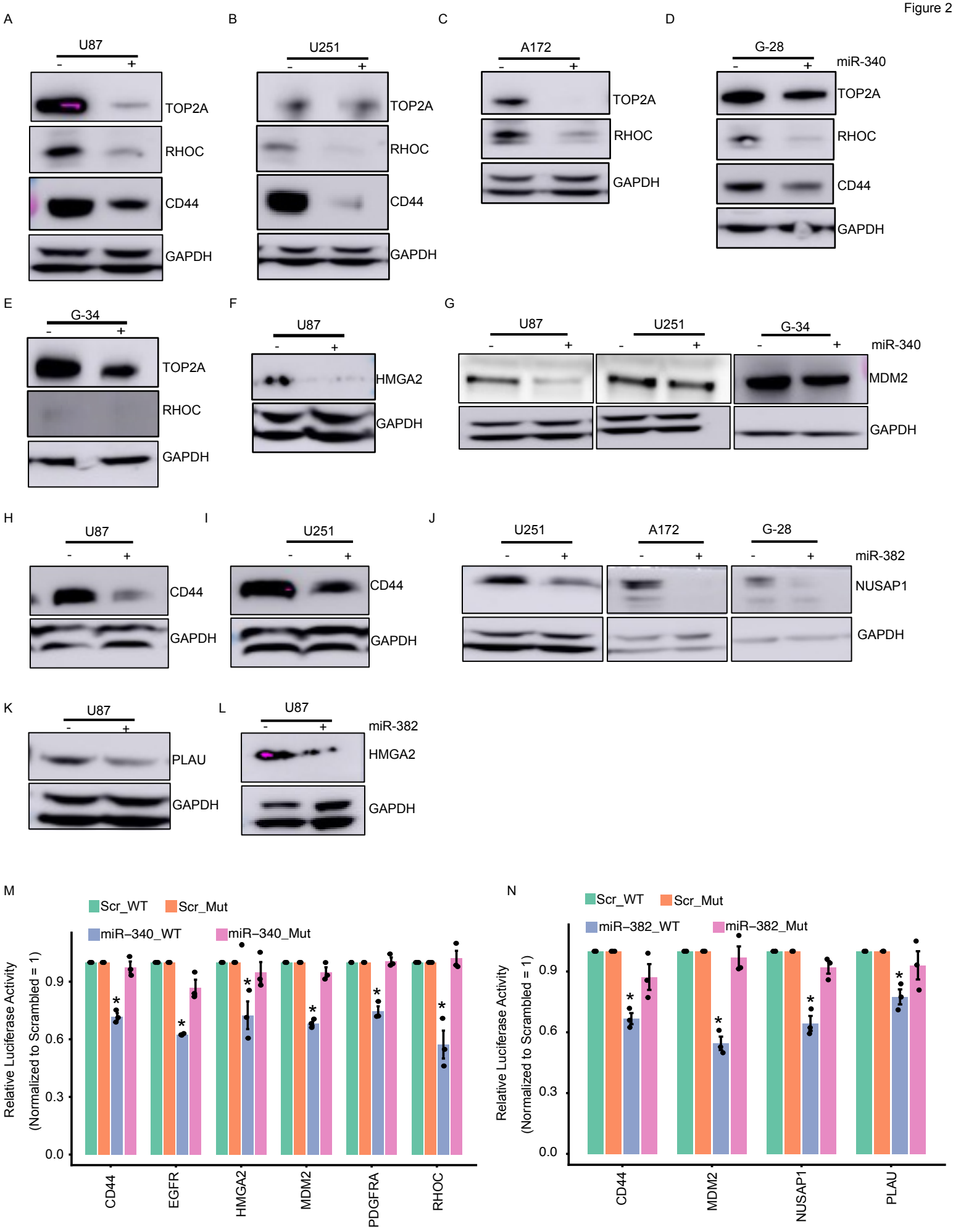
A
U87
- +
TOP2A
RHOC
CD44
GAPDH
B
U251
- +
TOP2A
RHOC
CD44
GAPDH
C
A172
- +
TOP2A
RHOC
GAPDH
D
G-28
- +
miR-340
TOP2A
RHOC
CD44
GAPDH
E
G-34
- +
TOP2A
RHOC
GAPDH
F
U87
- +
HMGA2
GAPDH
G
U87
U251
G-34
- + - + - +
miR-340
MDM2
GAPDH
H
U87
- +
CD44
GAPDH
I
U251
- +
CD44
GAPDH
J
U251
A172
G-28
- + - + - +
miR-382
NUSAP1
GAPDH
K
U87
- +
PLAU
GAPDH
L
U87
- +
miR-382
HMGA2
GAPDH
M
Scr_WT
Scr_Mut
miR−340_WT
miR−340_Mut
Relative Luciferase Activity
(Normalized to Scrambled = 1)
0.0
0.3
0.6
0.9
CD44
EGFR
HMGA2
MDM2
PDGFRA
RHOC
N
Scr_WT
Scr_Mut
miR−382_WT
miR−382_Mut
Relative Luciferase Activity
(Normalized to Scrambled = 1)
0.0
0.3
0.6
0.9
CD44
MDM2
NUSAP1
PLAU

A

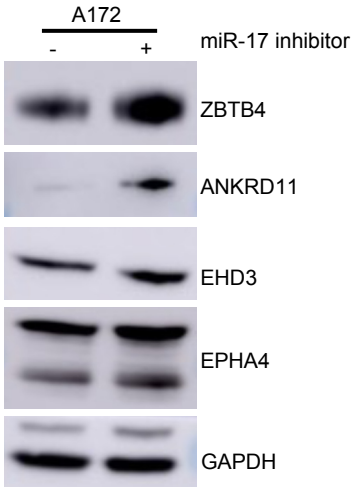
A172
- +
miR-17 inhibitor
ZBTB4
ANKRD11
EHD3
EPHA4
GAPDH

B

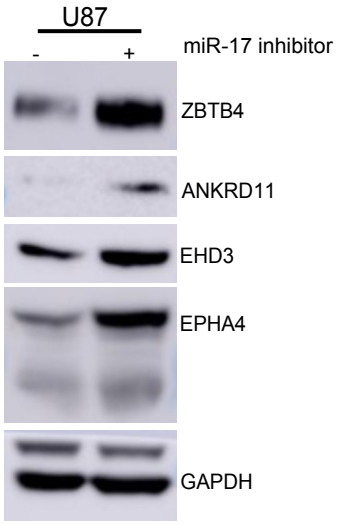
U87
- +
miR-17 inhibitor
ZBTB4
ANKRD11
EHD3
EPHA4
GAPDH

C

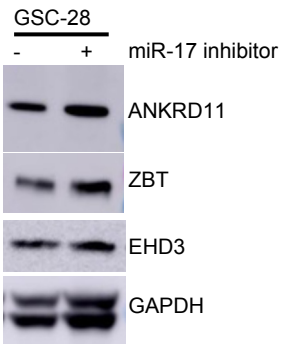
GSC-28
- +
miR-17 inhibitor
ANKRD11
ZBT
EHD3
GAPDH

D

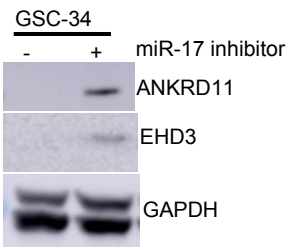
GSC-34
- +
miR-17 inhibitor
ANKRD11
EHD3
GAPDH

E

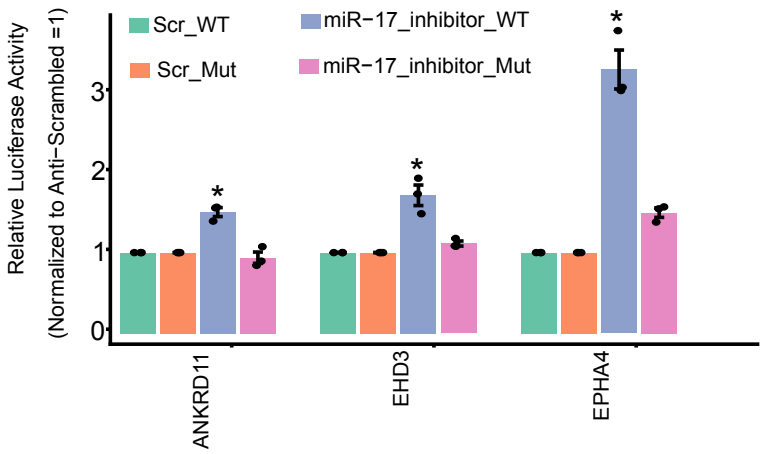
Relative Luciferase Activity
(Normalized to Anti−Scrambled =1)
Scr_WT
Scr_Mut
miR−17_inhibitor_WT
miR−17_inhibitor_Mut
0
1
2
3
*
*
*
ANKRD11
EHD3
EPHA4

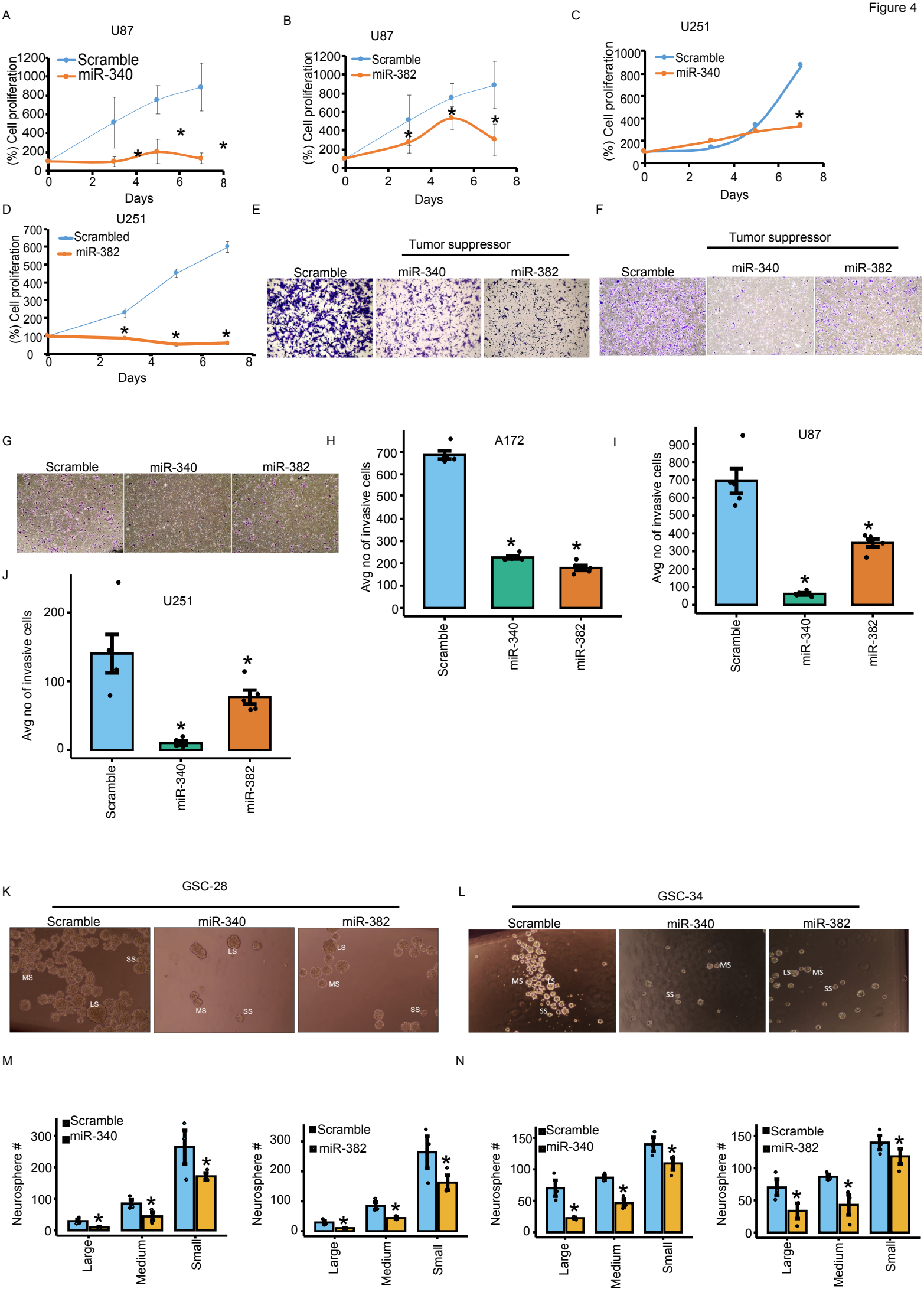
A
U87
Scramble
miR-340
(%) Cell proliferation
Days
B
U87
Scramble
miR-382
(%) Cell proliferation
Days
C
U251
Scramble
miR-340
(%) Cell proliferation
Days
D
U251
Scrambled
miR-382
(%) Cell proliferation
Days
E
Tumor suppressor
Scramble
miR-340
miR-382
F
Tumor suppressor
Scramble
miR-340
miR-382
G
Scramble
miR-340
miR-382
H
A172
Avg no of invasive cells
Scramble
miR-340
miR-382
I
U87
Avg no of invasive cells
Scramble
miR-340
miR-382
J
U251
Avg no of invasive cells
Scramble
miR-340
miR-382
K
GSC-28
Scramble
miR-340
miR-382
SS
MS
LS
L
GSC-34
Scramble
miR-340
miR-382
MS
LS
SS
M
Scramble
miR-340
Neurosphere #
Large
Medium
Small
Scramble
miR-382
Neurosphere #
Large
Medium
Small
N
Scramble
miR-340
Neurosphere #
Large
Medium
Small
Scramble
miR-382
Neurosphere #
Large
Medium
Small

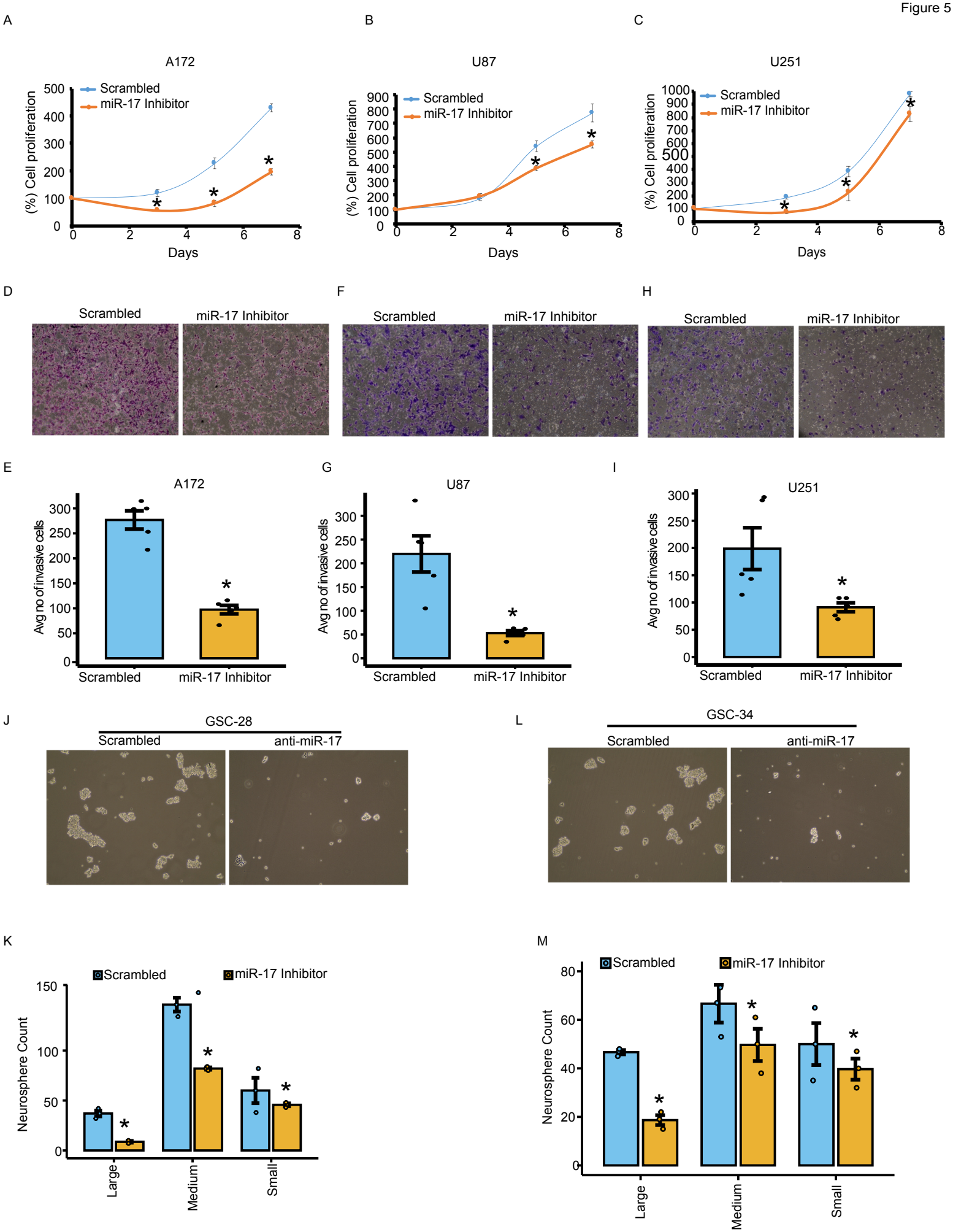
A
A172
Scrambled
miR-17 Inhibitor
(%) Cell proliferation
Days
B
U87
C
U251
D
F
H
E
Avg no of invasive cells
G
I
J
GSC-28
anti-miR-17
L
GSC-34
K
Neurosphere Count
Large
Medium
Small
M

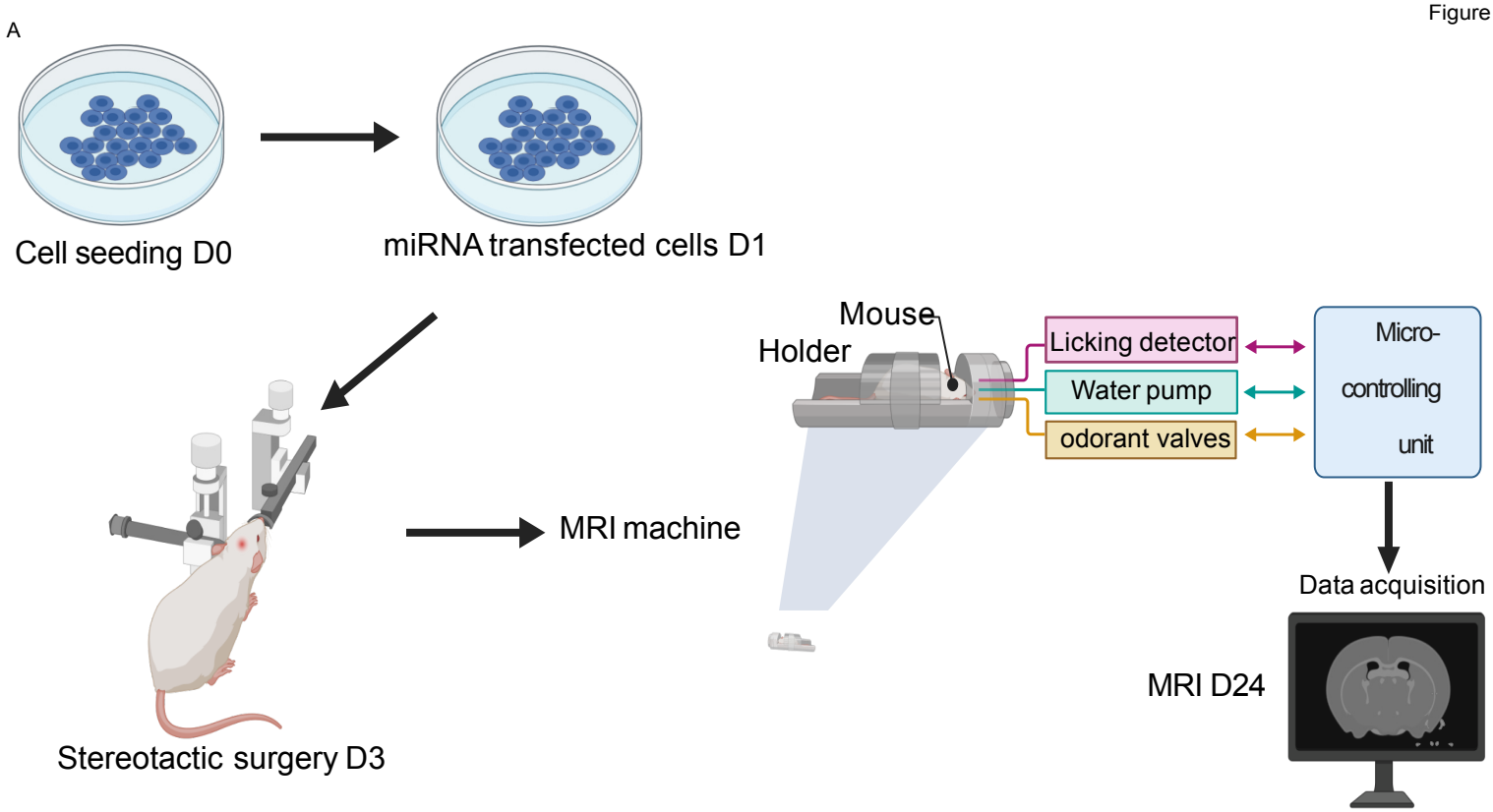
A
Cell seeding D0
miRNA transfected cells D1
Stereotactic surgery D3
MRI machine
Mouse
Holder
Licking detector
Water pump
odorant valves
Micro-
controlling
unit
Data acquisition
MRI D24

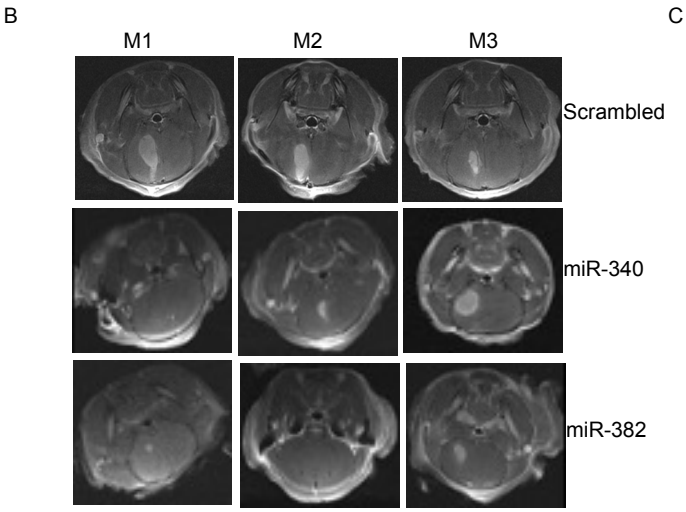
B
M1
M2
M3
Scrambled
miR-340
miR-382

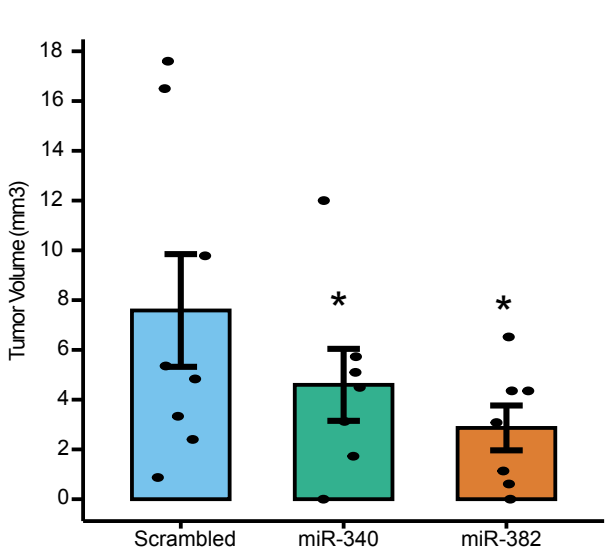
C
Tumor Volume (mm3)
0
2
4
6
8
10
12
14
16
18
*
*
Scrambled
miR-340
miR-382

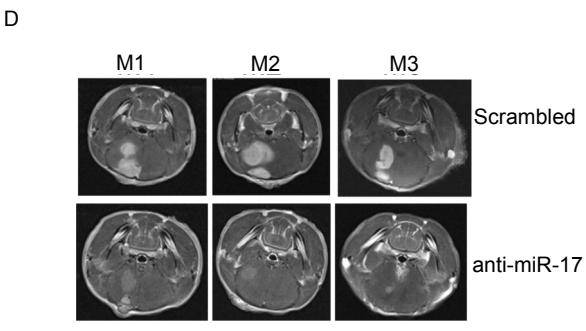
D
M1
M2
M3
Scrambled
anti-miR-17

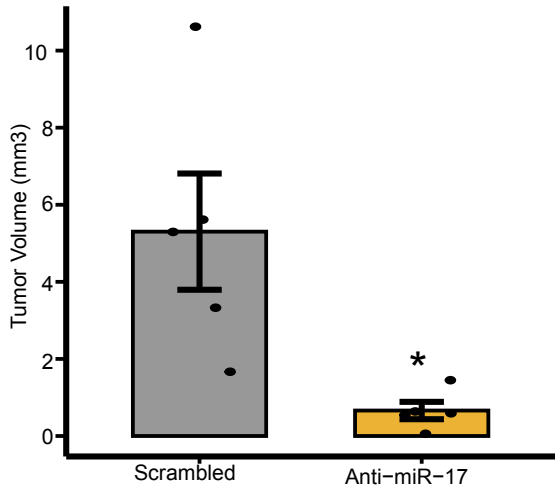
E
Tumor Volume (mm3)
0
2
4
6
8
10
*
Scrambled
Anti-miR-17

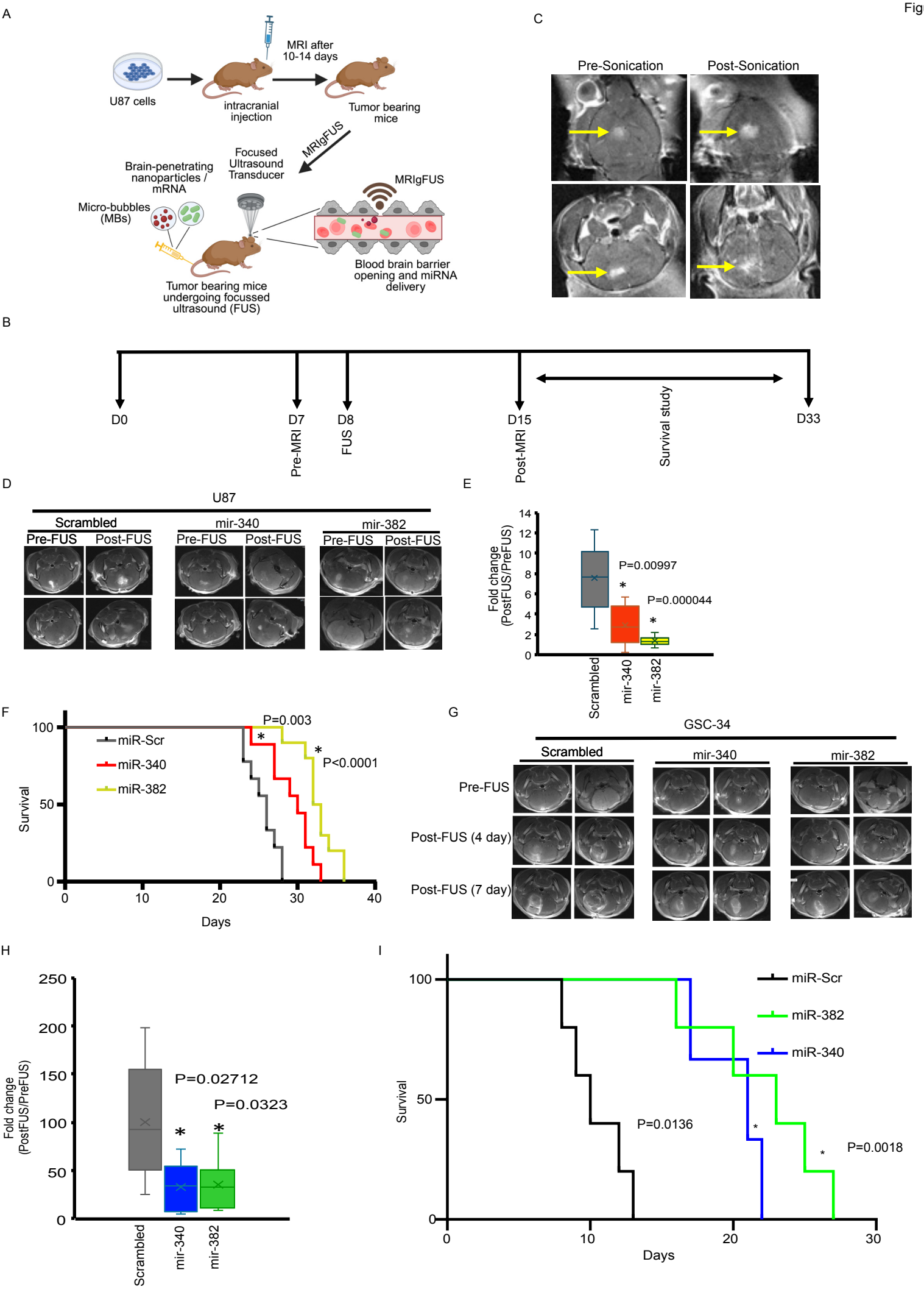
A
U87 cells
intracranial injection
MRI after 10-14 days
Tumor bearing mice
MRIgFUS
Focused Ultrasound Transducer
Brain-penetrating nanoparticles / mRNA
Micro-bubbles (MBs)
MRIgFUS
Blood brain barrier opening and miRNA delivery
Tumor bearing mice undergoing focussed ultrasound (FUS)
C
Pre-Sonication
Post-Sonication
B
D0
D7
Pre-MRI
D8
FUS
D15
Post-MRI
Survival study
D33
D
U87
Scrambled
mir-340
mir-382
Pre-FUS
Post-FUS
E
Fold change (PostFUS/PreFUS)
P=0.00997
P=0.000044
Scrambled
mir-340
mir-382
F
Survival
Days
miR-Scr
miR-340
miR-382
P=0.003
P<0.0001
G
GSC-34
Scrambled
mir-340
mir-382
Pre-FUS
Post-FUS (4 day)
Post-FUS (7 day)
H
Fold change (PostFUS/PreFUS)
P=0.02712
P=0.0323
Scrambled
mir-340
mir-382
I
Survival
Days
miR-Scr
miR-382
miR-340
P=0.0136
P=0.0018

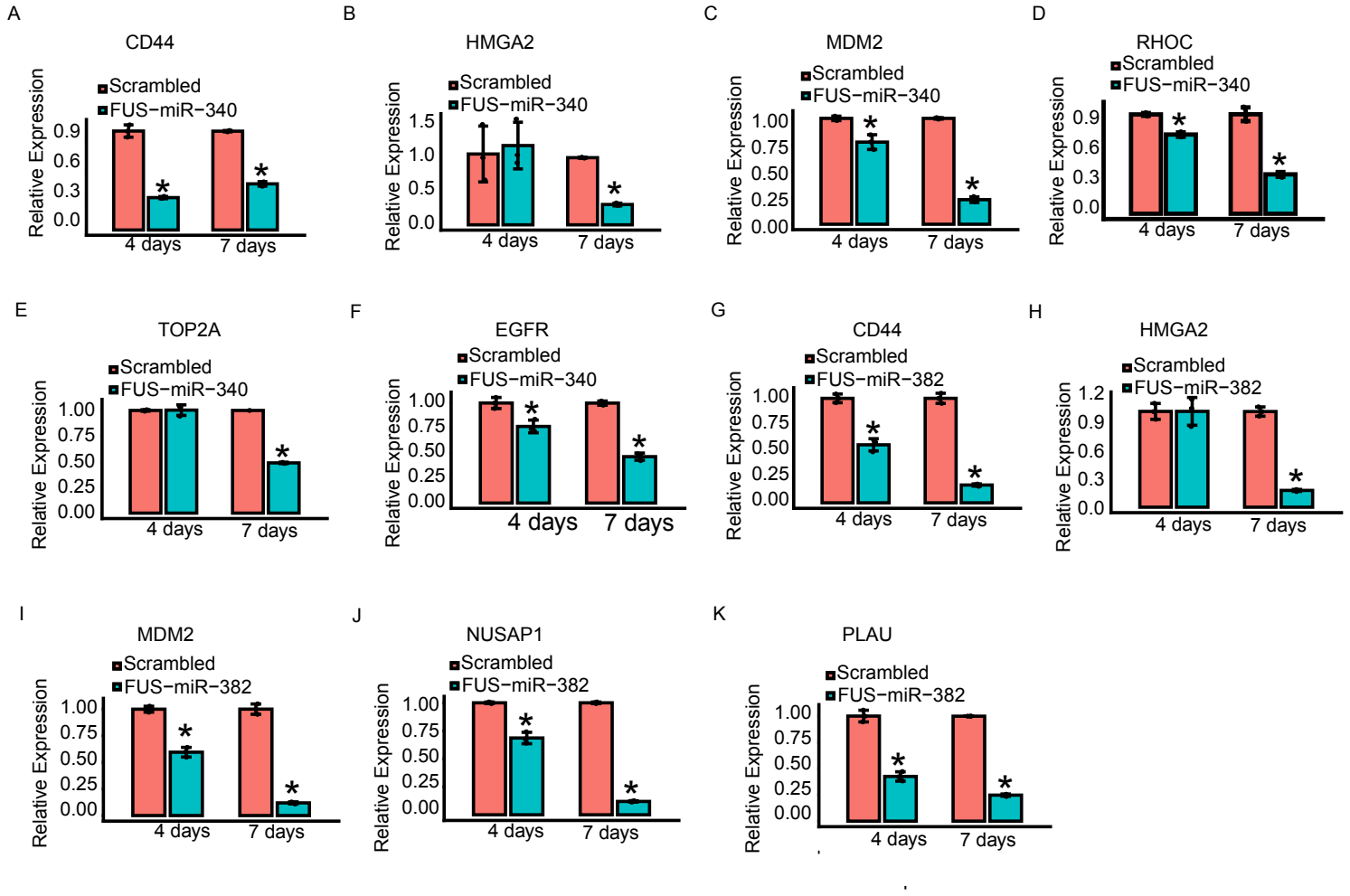
A
CD44
Scrambled
FUS-miR-340
Relative Expression
4 days
7 days
B
HMGA2
C
MDM2
D
RHOC
E
TOP2A
F
EGFR
G
CD44
Scrambled
FUS-miR-382
H
HMGA2
I
MDM2
J
NUSAP1
K
PLAU

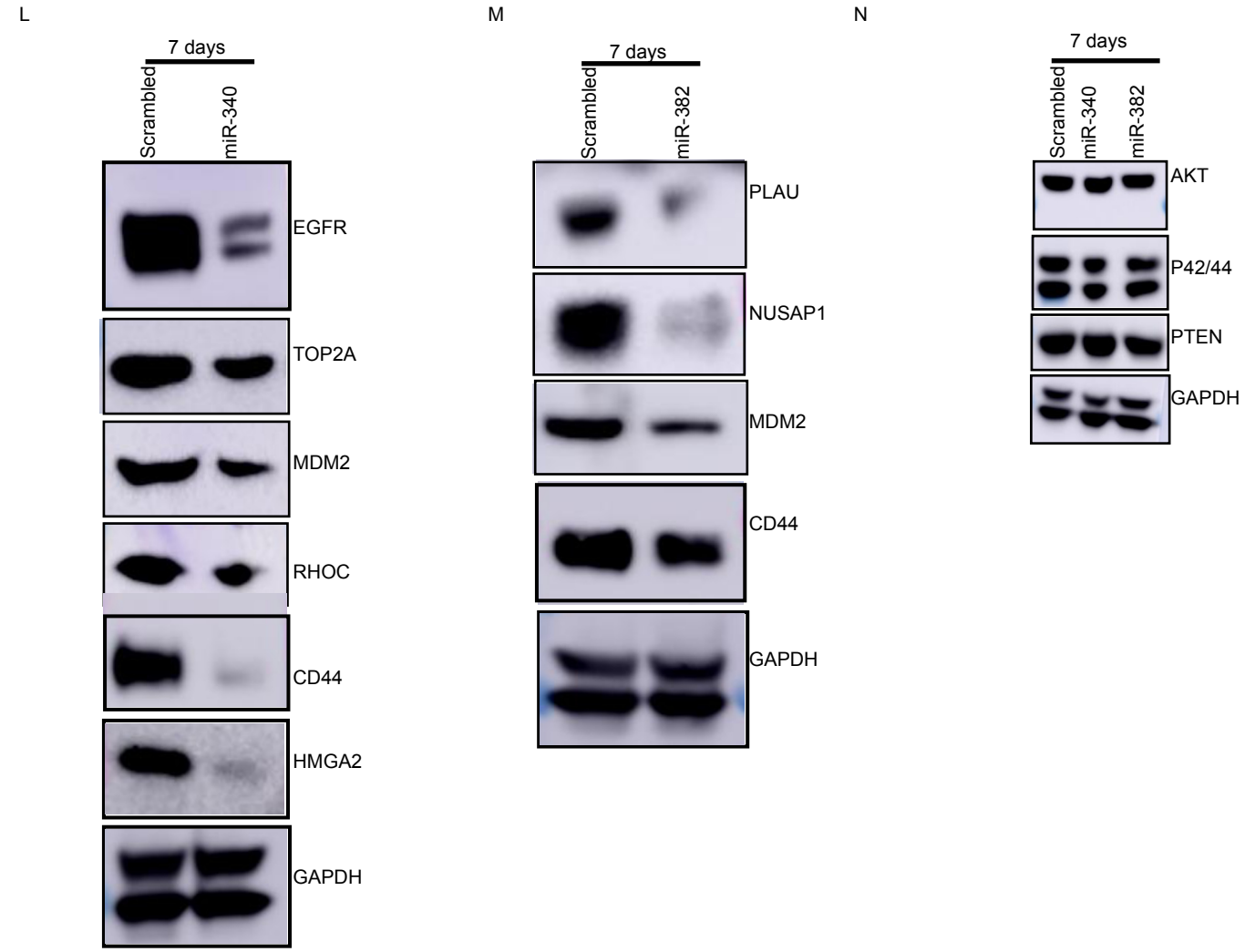
L
7 days
Scrambled
miR-340
EGFR
TOP2A
MDM2
RHOC
CD44
HMGA2
GAPDH
M
7 days
Scrambled
miR-382
PLAU
NUSAP1
MDM2
CD44
GAPDH
N
7 days
Scrambled
miR-340
miR-382
AKT
P42/44
PTEN
GAPDH